RESILIENCE-AWARE MANAGEMENT OF
ACTIVE DISTRIBUTION NETWORKS

by

Mohammad Alali

A thesis submitted in partial fulfillment
of the requirements for the degree

of

Master of Science

in

Electrical Engineering

MONTANA STATE UNIVERSITY
Bozeman, Montana

April 2021

DEDICATION

I dedicate this to everyone who has helped during completing my master's degree and guided me along this journey. I want to especially thank all my committee members who have lighten my path throughout my research. I also appreciate all the support and love I've received from my family and friends, which kept me going no matter what.

TABLE OF CONTENTS

TABLE OF CONTENTS CONTINUED

LIST OF TABLES

LIST OF FIGURES

LIST OF FIGURES CONTINUED

Figure Page

NOMENCLATURE

$\boldsymbol{DSS}$	Distributed Storage System
$\boldsymbol{t}$	Time
$\boldsymbol{i,j}$	Index of nodes
$\boldsymbol{V_{i,t}}$	Voltage of bus $\boldsymbol{i}$ at time $\boldsymbol{t}$
$\boldsymbol{V_{ref}}$	Magnitude of the reference voltage
$\boldsymbol{W_{vol}}$	Weight coefficient of voltage minimization
$\boldsymbol{W_{loss}}$	Weight coefficient of loss minimization
$\boldsymbol{\Gamma_{loss}}$	Network losses
$\boldsymbol{Res_{index}}$	Resiliency Index
$\boldsymbol{W_{res}}$	Weight coefficient of Resiliency Index minimization
$\boldsymbol{F_{GA}}$	Value of fitness function
$\boldsymbol{C_t^E}$	Cost of energy from the grid at time $\boldsymbol{t}$
$\boldsymbol{E_t}$	Energy flow towards an external grid
$\boldsymbol{\eta_i}$	DSS energy efficiency
$\boldsymbol{E_{DSS_i}^0}$	Initial energy stored in all DSSs connected to $\boldsymbol{i^{th}}$ bus
$\boldsymbol{E_{DSS_i}^{max}}$	Maximum capacity of the DSS reservoir connected to the $\boldsymbol{i^{th}}$ bus
$\boldsymbol{E_{DSS_i}^{min}}$	Minimum capacity of the DSS reservoir connected to the $\boldsymbol{i^{th}}$ bus
$\boldsymbol{E_{DSS_i}^t}$	Energy stored in the DSS connected to $\boldsymbol{i^{th}}$ bus at time $\boldsymbol{t}$
$\boldsymbol{P_{DSS_i}^{max}}$	Maximum power capability of the DSS connected to the $\boldsymbol{i^{th}}$ bus
$\boldsymbol{P_{DSS_i}^{min}}$	Minimum power capability of the DSS connected to the $\boldsymbol{i^{th}}$ bus
$\boldsymbol{P_{DSS_i}^t}$	Active power produced/absorbed by the DSS connected to $\boldsymbol{i^{th}}$ bus at time $\boldsymbol{t}$

NOMENCLATURE CONTINUED

$\boldsymbol{Q^{t}_{DSS_i}}$	Reactive power produced/absorbed by the DSS connected to $\boldsymbol{i^{th}}$ bus at time $\boldsymbol{t}$
$\boldsymbol{Q_{L_{i,j}}}$	Reactive power absorbed at $\boldsymbol{i^{th}}$ bus at time $\boldsymbol{t}$
$\boldsymbol{Q_{G_{i,t}}}$	Reactive power generated at $\boldsymbol{i^{th}}$ bus at time $\boldsymbol{t}$
$\boldsymbol{P_{l_{i,t}}}$	Active power absorbed at $\boldsymbol{i^{th}}$ bus at time $\boldsymbol{t}$
$\boldsymbol{P_{G_{i,t}}}$	Active power generated at $\boldsymbol{i^{th}}$ bus at time $\boldsymbol{t}$
$\boldsymbol{\delta_{i,t}}$	Voltage phase of bus $\boldsymbol{i}$ at time $\boldsymbol{t}$
$\boldsymbol{G_{i,j}}$	Conductance of the line between buses $\boldsymbol{i}$ and $\boldsymbol{j}$
$\boldsymbol{B_{i,j}}$	Susceptance of the line between buses $\boldsymbol{i}$ and $\boldsymbol{j}$
$\boldsymbol{C^{max}_{DSS_i}}$	Power capability limit of the DSS connected to the $\boldsymbol{i^{th}}$ bus
$\boldsymbol{Z}$	Impedance of the transmission line between the DGs
$\boldsymbol{i,j}$	Index of nodes
$\boldsymbol{V_i}$	Voltage of $\boldsymbol{DG_i}$
$\boldsymbol{\delta_i}$	Phase of $\boldsymbol{DG_i}$
$\boldsymbol{P}$	Real power of the inverter
$\boldsymbol{Q}$	Reactive power of the inverter
$\boldsymbol{\widetilde{P}}$	Instantaneous real power of the inverter
$\boldsymbol{\widetilde{Q}}$	Instantaneous reactive power of the inverter
$\boldsymbol{P_{ir}}$	Real power reference for inverter i
$\boldsymbol{Q_{ir}}$	Reactive power reference for inverter i
$\boldsymbol{\omega_c}$	Value of fitness function
$\boldsymbol{V_{i,abc}}$	Voltage of node i in ***abc*** reference frame
$\boldsymbol{V_{i,dq}}$	Voltage of node i in ***dq*** reference frame
$\boldsymbol{i_{j,abc}}$	Current of node j in ***abc*** reference frame
$\boldsymbol{i_{j,abc}}$	Current of node j in ***dq*** reference frame
$\boldsymbol{V^{*}}$	Output voltage of the power controller Used as

NOMENCLATURE CONTINUED

	a reference voltage for the IMC voltage controller
$\boldsymbol{\omega}^*$	Output frequency of the power controller Used as a reference frequency for the IMC voltage controller
$\boldsymbol{\omega_{pll}}$	Angular frequency of the PLL
$\boldsymbol{\omega_n}$	Reference angular frequency
$\boldsymbol{V_n}$	Reference voltage
$\boldsymbol{\omega_i}$	Angular frequency of the inverters
$\boldsymbol{L_i}$	Inductors used in the lowpass filter
$\boldsymbol{r_i}$	Resistors used in the lowpass filter
$\boldsymbol{R_d}$	Used to model the capacitor's series resistance
$\boldsymbol{C_f}$	Capacitor of the lowpass filter
$\boldsymbol{K_{pv}}$	The coefficient for the proportional controller related to the voltage controller
$\boldsymbol{K_{iv}}$	The coefficient for the integral controller related to the voltage controller
$\boldsymbol{K_{dv}}$	The coefficient for the derivative controller related to the voltage controller
$\boldsymbol{K_{pc}}$	The coefficient for the proportional controller related to the current controller
$\boldsymbol{K_{ic}}$	The coefficient for the integral controller related to the current controller
$\boldsymbol{K_{dc}}$	The coefficient for the derivative controller related to the current controller
$\boldsymbol{K_{pd}(s)}$	Transfer function of the PD controller in the internal model-based controller
$\boldsymbol{K_{pi}(s)}$	Transfer function of the PI controller in the internal model-based controller

NOMENCLATURE CONTINUED

$\boldsymbol{K_{pid}(s)}$	Transfer function of the PID controller in the internal model-based controller
$\boldsymbol{\lambda_v}$	Tuning parameter for the IMC voltage controller
$\boldsymbol{\lambda_c}$	Tuning parameter for the IMC current controller
$\boldsymbol{T_c}$	Time period of the inverter output signal
$\boldsymbol{T_{pwm}}$	Time period of the inverter switching
$\boldsymbol{\phi_i}$	States of the IMC voltage controller
$\boldsymbol{\gamma_i}$	States of the IMC current controller
$\boldsymbol{V_{bDi}}$	Input voltage in d-axis
$\boldsymbol{V_{bQi}}$	Input voltage in q-axis
$\boldsymbol{R_N}$	Virtual resistor
$\boldsymbol{m}$	One of the Control parameters of the power controller used to control the voltage
$\boldsymbol{n}$	One of the Control parameters of the power controller used to control the frequency
$\boldsymbol{K_e}$	One of the Control parameters of the power controller
$\boldsymbol{f_{sw}}$	Inverter’s switching frequency

ABSTRACT

The electric power system is one of the greatest engineering achievements in the history of mankind. Electricity is integral to every part of our economy and society. Therefore, it is essential to make the electricity grid more resilient in facing different extreme events and black outs. In this work, four problems have been investigated to study and improve the resiliency of distribution networks. The first one focuses on the problem of power line congestion which can negatively harm the economy and different equipment in the grid. Two neural network models are used to predict where the congestion might happen and what would be the cause of it. Using these predictions, the problem can be alleviated in time and the resiliency of the grid will be improved. The second problem discusses power management of the distribution network under the occurrence of an extreme event. The problem is formulated as a Markov Decision Process using different agents and is solved using two Reinforcement Learning algorithms, namely, Q-Learning and Value Iteration. This approach is then tested on a benchmark system and the results show a remarkable improvement of the resiliency. The third problem studies the stability and power sharing of parallel inverters in a multi inverter-fed system. A small signal model of the power controller is studied. Further, the system's nonlinear dynamic equations are derived using accurate mathematical models. The system model is then trimmed and linearized around its operating point and the system's control parameters are optimized using Grey Wolf Optimization. Finally, improvement of stability and power sharing are verified by running time domain simulations. The last problem investigates the optimal siting and sizing of energy storage systems in a multi-microgrid system to improve the resiliency. A two-stage optimization method is used to solve the nonlinear and non-convex problem. The first stage involves an Optimal Power Flow and the second stage uses Genetic Algorithm. Further an investment cost based on the sensitivity analysis is introduced to improve the resiliency even further. The effectiveness of this ESS placement is tested on a benchmark system and validated using a fault scenario.

CHAPTER ONE

INTRODUCTION

The electric power system is one of the greatest engineering achievements in the history of mankind. Electricity is integral to every part of our economy and society. To remain reliable, our electricity grid must be revitalized with a new generation of infrastructure and investment. According to the international energy agency, the American power sector will need 2.1 trillion dollars of investment between now and the year 2035. Of course, we need to install more than steel and copper infrastructures to make our grid more connected, flexible, and resilient so it can integrate a new generation of cleaner, increasingly dispersed, and intermittent power sources, such as wind and solar. We must also protect the grid against new risks like cyber-attacks and extreme weather events. Besides a knowledge of the grid's physical laws, a profound understanding of data communication and analytics will also be needed to provide data-driven insights that are essential for the system optimization.

Today’s power grid consists of three general sections: 1) Generation which is responsible for generating the power and electricity. 2) Transmission, that transmits the power to the distributers and 3) Distribution which distributes the power to the consumers. These general sections are shown in Fig. 1. The main focus of this thesis is on the resiliency of the distribution part of the power system.

Resiliency is the ability of the system to withstand extreme events and recover rapidly with minimum damage. It features, maintaining stability by fast restoration, adapting strategy for future events, prediction of extreme events and minimizing their impacts. I’m sure we all remember the

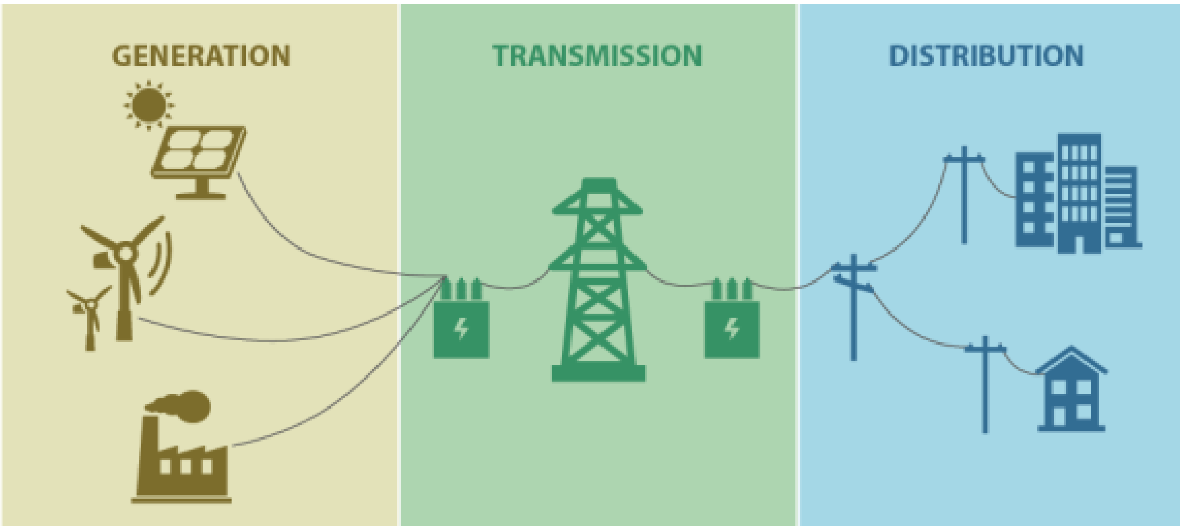

Fig. 1. General Sections of Today's Power Systems [6]

disastrous outage that happened in Texas on Feb 2021 which affected millions of people's lives and had consequences that would take years to recover (Fig. 2.). The total costs of this disaster were estimated to be 295 billion dollars. But this was not the first time that something like this has happened before, and it sure will not be the last. Besides severe weather there are many other causes like Vandalism, Equipment Failure, etc. that might lead to power outages. So, we need to be prepared and improve the resiliency of our grid. Moreover, competitive power markets are replacing monolithic regulated public utilities; and this, changes power system operation and regulation [1]. Due to the deregulation of power system and to be most cost-effective, distribution systems usually operate close to their maximum power transfer capability. Hence, distribution lines may operate near or exceed their maximum operating limits. This makes the distribution grid more vulnerable to disturbances and negatively impacts the reliability and resiliency of the distribution system [2], [3].

One of the ways to enhance the resiliency of the power system is Microgrid (MG) formation. Microgrid is an independent Anthonomus power system that can operate in both connected and islanded modes to provide efficient, resilient, reliable and clean energy [4], [5]. On the other hand, with the growing penetration of renewable energy resources, the distribution system is imposed to increasing uncertainty and intermittency; therefore, the grid's stability and operation is becoming more important. Due to the distributed characteristic of these generations, MGs are formed as decentralized group of generation units and loads. Unlike traditional utility grids, which have large synchronous generators, MGs consist of low inertia components. Therefore, control and stability issues in MGs are more important especially in an island mode. Different parts of a microgrid are shown in Fig. 3. As can be seen a microgrid can be combination a of different components such as generators, storage systems and different consumers. Other ways to improve the resiliency include distributed generation scheduling, responsive energy storage system, and demand response and load curtailment.

(a) (b)

Fig. 2. (a) Before Texas Outage; (b) After Texas Outage [7]

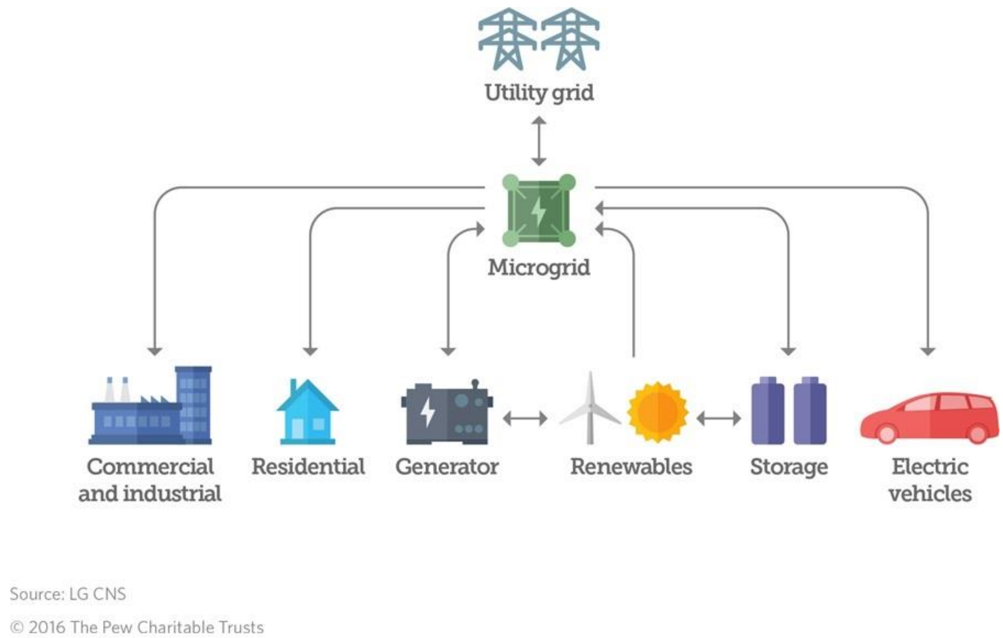

Fig. 3. Microgrid Components

In this work, four problems have been investigated to study and improve the resiliency of distribution networks:

The first problem in chapter 2 focuses on predicting power line congestion in active distribution networks which can happen in different cases such as during peak electricity consumption. Congestion can negatively affect the economy and different equipment in the grid. Consequently, it is essential to accurately predict congestions in a grid and resolve the issue fast.

Active distribution network is an electricity network that has systems in place to monitor and control the electricity grid. So, we have access to a very valuable asset, which is *Data*!

Many organizations have already been making different predictions based on various data. Amazon products page, Netflix shows, or Google ads which all show recommendations based on the browsing history. Our colleagues in the data science community have developed different kinds of prediction models which can use a finite amount of data to be trained and make accurate predictions. As an example, one of these models called neural networks have shown an outstanding performance in predicting the behavior of the electric power systems.

Therefore, in chapter 2, I propose a prognosis method with two neural network models. The first one will give a prediction of where the congestion would be and the second one will predict the cause of it. To test the effectiveness of this approach, I simulated and tested my method on a small power system, and the obtained results were remarkable. By knowing where the problem is and what is causing it, we can alleviate the problem in time and command proper control actions. I believe by utilizing my proposed method on a larger scale, we could make our electricity grid more reliable and we can avoid more catastrophic events.

Section I in chapter 2 provides a literature review of the subject; section II provides a detailed description of the neural network training algorithm and the general scheme used for the congestion predictions. In section III the training process of the NNs is described and improvement of the NN accuracy as per each iteration is illustrated. Further in this section, the trained neural networks are examined, and the results are presented based on two datasets; also, two indices are introduced to determine the performance of the proposed method. Finally, main conclusions and discussions of the future work are presented in section IV.

Chapter 3 presents power management of the distribution network under the occurrence of an extreme event. I aim to increase the resiliency of the system by adapting strategies for future event and minimizing the impacts. The power management problem is formulated as a Markov Decision Process using different agents. Then the problem is solved using two Reinforcement Learning algorithms, namely, Q-Learning and Value Iteration. This approach is then tested on a benchmark MG system and the results show a noticeable improvement of the resiliency.

Chapter 4 aims to improve the resiliency of a distributed generation system by focusing on the power electronic layer of the system. In this work, the stability, resiliency, and power sharing characteristics of IDGs comprising of a droop control with a secondary control loop and an IMC-based voltage and current controller is studied. Accurate mathematical modeling and equations of each of the mentioned components along with PLL, and the network and load models are discussed. The equations are then modeled using MATLAB, SIMULINK, after which an operating point is derived, and the equations are linearized around that operating point using the Linear Analysis Tool. The state space equations of the system are presented and the eigenvalue and sensitivity analysis of the IDG are presented using the system matrix (A). The critical parameters are identified, and stability domains of these parameters are presented. Moreover, a GWO algorithm is proposed to find the optimal control parameters and to improve the stability, resiliency, and power sharing in the system. Various load disturbances are applied in different time steps to show the effectiveness of the proposed GWO algorithm in the time domain simulations. Finally, different stability indices are calculated to verify the stability and resiliency of the DG system.

At first a comprehensive literature review is included in Section I of chapter 4. Section II provides a detailed description of mathematical modeling and equations of the MG components. In section III, the linearization and state space equations of the MG system is discussed in detail. In section IV, eigenvalue, and sensitivity analysis of the MG system are investigated. Furthermore, critical control parameters of each component are recognized, and the parameter stability domains are presented. After which, the optimal control parameters are derived using GWO. Section V presents the simulation results and performance evaluation of the optimal parameters. Finally, main conclusions and discussions of the future work are presented in section VI.

Chapter 5 includes the problem of optimal siting and sizing of energy storage systems in a multi-microgrid system to improve the resiliency. Specifically, this study discusses a planning optimization problem relating to siting and sizing of the ESSs with the goal of minimizing the network loss and energy cost from the grid in a multi-microgrid system. The mentioned problem is a mixed-integer, nonlinear and non-convex problem. Due to the complexity of this problem, a two-stage process is introduced. The two stage iterative process consists of two parts: (i) the first part, a GA algorithm is used to find the site and size of the ESS units (ii) in the second stage, the fitness of the first part is evaluated using an AC-OPF. A benchmark multi-microgrid system is studied to show the effectiveness of the proposed method to find the optimal allocation of the ESSs. In this study, loads and PV absorption and generation has been considered for a winter day. Also, two investment costs are considered for the simulation: one constant and another one based on the voltage sensitivity analysis. A fault scenario is also examined to verify the performance of the ESSs' siting and sizing.

Section 1 of chapter 5 goes over the literature related to the topic. Section II provides a detailed description of the problem formulation. In section III, the benchmark multi-microgrid system is introduced and the suggested planning of the ESSs is investigated on this system considering a constant investment cost. The obtained results from the proposed optimization method are presented using different tables and figures. Further, an investment cost is introduced based on the sensitivity analysis of the MGs and the improvement of the resiliency is demonstrated.

Also, a fault scenario is investigated to show the effectiveness of the optimal planning of the batteries. Finally, main conclusions and discussions of future work are presented in in section IV.

References

[1] A. Chaouachi, R. Kamel, R. Andoulsi, and K. Nagasaka, “Multiobjective intelligent energy management for a microgrid,” *IEEE Trans. Indust. Elec.*, vol. 60 pp. 1688–1699, Apr. 2013.

[2] R. Lasseter, “Microgrids,” *Proc. IEEE Power Eng. Society Trans. and Dist. Conf.*, vol. 1, pp. 305 – 308, Jan. 2002.

[3] C. Schwaegerl, “Advanced architectures and control concepts for more microgrids, *More Microgrids, Siemens AG, STREP*, no. 1, pp. 1–145, 2009.

[4] I. T. Force *et al.*, “Trends in Microgrid Control,” vol. 5, no. 4, pp. 1905–1919, 2014.

[5] R. Majumder, “Some Aspects of Stability in Microgrids,” vol. 28, no. 3, pp. 3243–3252, 2013.

[6] CRS, adapted from U.S.-Canada Power System Outage Task Force, Final Report on the August 14, 2003, Blackout in the United States and Canada: Causes and Recommendations, April 2004, p.5, https://www.energy.gov/sites/prod/files/oeprod/DocumentsandMedia/BlackoutFinal-Web.pdf.

[7] https://earthobservatory.nasa.gov/images/147941/extreme-winter-weather-causes-us-blackouts

CHAPTER TWO

INTELLIGENT LINE CONGESTION PROGNOSIS IN ACTIVE DISTRIBUTION SYSTEM USING ARTIFICIAL NEURAL NETWORK

Contribution of Authors and Co-Authors

Manuscript in Chapter Two

Author: Mohammad Alali

Contributions: Chose the suitable neural network models as the prediction model and trained them according to the defined problem, generated a training set, generated the figures and test cases, prepared most of the manuscript.

Co-Author: Farshina Nazrul Shimim

Contributions: Aided in the literature review, preparing some of the dataset for training the neural networks, aided in analyzing the data.

Co-Author: Dr. Zagros Shahooei

Contributions: Provided important insight and overview of the problem, interpretation of results, and aided in the preparation and editing of the manuscript and figures.

Co-Author: Dr. Maryam Bahramipanah

Contributions: Suggested the main idea, provided important insight and overview of the problem, interpretation of results, and aided in the preparation and editing of the manuscript and figures.

Manuscript Information

Mohammad Alali, Farshina Nazrul Shimim, Zagros Shahooei, Maryam Bahramipanah

2021 IEEE Power & Energy Society Innovative Smart Grid Technologies Conference (ISGT)

Status of Manuscript:

____ Prepared for submission to a peer-reviewed journal
____ Officially submitted to a peer-reviewed journal
____ Accepted by a peer-reviewed journal
_X_ Published in a conference proceeding

Publisher: IEEE

Published on IEEE *Xplore* Digital Library
DOI: 10.1109/ISGT49243.2021.9372244

Intelligent Line Congestion Prognosis in Active Distribution System Using Artificial Neural Network

Mohammad Alali, Farshina Nazrul Shimim, Zagros Shahooei, Maryam Bahramipanah
Department of Electrical and Computer Engineering,
Montana State University, Bozeman, MT

2021 IEEE Power & Energy Society Innovative Smart Grid Technologies Conference (ISGT) | 978-1-7281-8897-3/21/$31.00 ©2021 IEEE | DOI: 10.1109/ISGT49243.2021.9372244

***Abstract*—This paper proposes an intelligent line congestion prognosis scheme based on wide-area measurements, which accurately identifies an impending congestion and the problem causing the congestion. Due to the increasing penetration of renewable energy resources and uncertainty of load/generation patterns in the Active Distribution Networks (ADNs), power line congestion is one of the issues that could happen during peak load conditions or high-power injection by renewable energy resources. Congestion would have devastating effects on both the economical and technical operation of the grid. Hence, it is crucial to accurately predict congestions to alleviate the problem in-time and command proper control actions; such as, power redispatch, incorporating ancillary services and energy storage systems, and load curtailment. We use neural network methods in this work due to their outstanding performance in predicting the nonlinear behavior of the power system. Bayesian Regularization, along with Levenberg-Marquardt algorithm, is used to train the proposed neural networks to predict an impending congestion and its cause. The proposed method is validated using the IEEE 13-bus test system. Utilizing the proposed method, extreme control actions (i.e., protection actions and load curtailment) can be avoided. This method will improve the distribution grid resiliency and ensure the continuous supply of power to the loads.**

***Index Terms*—Fault Prognosis, Line Congestion, Resiliency, Neural Networks, Levenberg-Marquardt, Bayesian Regularization**

I. Introduction

Nowadays, we are more dependent on electric energy than ever. On the other hand, with the growing penetration of renewable energy resources, the distribution system is imposed to increasing uncertainty and intermittency. Moreover, competitive power markets are replacing monolithic regulated public utilities; and this, changes power system operation and regulation [1]. Due to the deregulation of power system and to be most cost-effective, distribution systems usually operate close to their maximum power transfer capability. Hence, distribution lines may operate near or exceed their maximum operating limits. This makes the distribution grid more vulnerable to disturbances and negatively impacts the reliability of the distribution system [2], [3]. It is hence critical to predict the impending congestions to minimize load curtailments and ensure fast recovery from a disturbance. Congestions in distribution system should be mitigated very fast to ensure the safe and normal operation of the system and avoid any resulting or cascading failures. By fast detection of impending congestion in an Active Distribution Network (ADN), proper preventive control actions can be taken to alleviate the problem and prevent further contingencies. Hence, fast and accurate congestion detection, will help to improve the grid resiliency.

Generally, constraints such as load level and thermal limits of the distribution lines are considered as a scheduling optimization problem to properly schedule all the generation units for the next day or hour. However, due to the highly nonlinear characteristics of the distribution system, especially with intermittent renewable resources, these constraints may change very quickly or be violated in practice. Therefore, it is crucial to monitor the distribution system and predict line congestions to avoid the harmful consequences such as load curtailment and damages to equipment [4].

There are two different strategies to mitigate congestion in an ADN: grid reinforcement, and active management strategies. Grid reinforcement is a long-term solution and refers to installing new distribution lines and generation units. Active management strategies are performed during distribution system operation and include generation rescheduling, on-load tap changers, flexible AC transmission system (FACTS) devices, incentive-price-based demand response, transaction and auction techniques, load curtailment, and etc. [3], [5], [6]. However, it is very important to predict an impending congestion and decrease congestion risks in a cost-efficient way instead of mitigating congestion in an ADN.

In [7], a congestion relief problem in a transmission system is investigated considering generation cost and demand interruption cost for N-1 contingency criteria. Further, different components such as energy storage devices and uncertain renewable energy sources are considered and the non-linear problem is solved using GAMS. [8] and [9] propose a demand response approach for the congestion management problem in distribution systems. Furthermore, [10] discusses the increasing need for the cooperation between the distribution system operators and transmission system operators, and proposes some solutions for distribution congestion management problem.

Data-driven methods such as Neural Networks (NNs) are also introduced as alternative solutions for congestion management and prevention. NNs have a wide range of applications in power system monitoring, analysis, control, and protection such as load forecasting, economic dispatch, and

978-1-7281-8897-3/21/$31.00 ©2021 IEEE

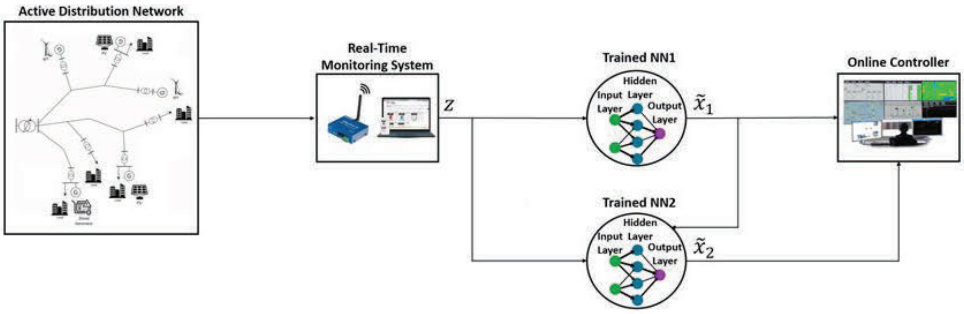

Fig. 1. General Scheme of the Intelligent Congestion Prognosis

fault diagnosis. Among the various architectures associated with NNs, Feed-Forward Neural Network (FNN) is very popular due to its simplicity and high accuracy rate. NNs could also be used to predict line overloading. Sharma et al. [11] presents a Cascade Neural Network (CNN) approach to identify the overloaded transmission lines and then predict the amount of overloading in a transmission line. In [12], Artificial Neural Network (ANN) is used instead of classical estimation algorithms to predict different states of transmission and distribution system. Further in [13] a Multilayer Perceptron Neural Network is utilized for state estimation of a power system. Fainti et al. [14] use ANN to predict congestion in each phase of a three-phase distribution system; however, they assume that congestion only occurs in the first bus where the main feeder is connected to the grid. Moreover, their method does not identify the cause of congestion; so, the provided information does not help the system operator to perform corrective control actions to mitigate the problem.

In this paper, we propose a novel intelligent scheme to predict line congestions in ADNs which will help to improve the grid resiliency. Our proposed method overcomes the inherent nonlinear and nonconvex behavior of distribution system and congestion management problem. We introduce an intelligent congestion prognosis scheme utilizing two NNs. Our proposed method is capable of predicting line congestions in an ADN, where overloading can occur in more than one line. We are using congestion detection as a way to prevent overloading on the lines. Further, our method identifies the cause of the congestion as well and this will guide the grid operators to perform proper preventive actions to mitigate the problem. With the proposed method, we can deal with small disturbances such as load increase or dynamic changes of the system without any extreme control actions such as load curtailment and this will help to improve the distribution system resiliency.

The remainder of this paper is organized as follows. Section II provides a detailed description of the neural network training algorithm and the general scheme used for the congestion predictions. In section III the training process of the NNs is described and improvement of the NN accuracy as per each iteration is illustrated. Further in this section, the trained neural networks are examined, and the results are presented based on two datasets; also, two indices are introduced to determine the performance of the proposed method. Finally, main conclusions and discussions of the future work are presented in section IV.

II. METHODOLOGY

Unlike transmission system, distribution systems generally lack real-time measurement and control technologies; hence, they include large unmonitored areas and, most of their measurements are not synchronized. Usually, distribution management systems rely on two approaches: 1) local measurements provided by Supervisory Control and Data Acquisition (SCADA); 2) Phasor Measurement Units (PMUs), which are limited due to the few number of installations. Different state estimation techniques are commonly used for distribution network monitoring. However, due to specific characteristics of distribution systems such as, relatively high R/X ratio, radial design, three-phase imbalance, unmonitored states for switches and regulators, incomplete load/generation information, and limited number of measurements, pseudo-measurement of unmonitored buses might not be accurate and this will lead to wrong state estimations. In addition, these challenges get worse by the changing dynamics of the distribution network and its growing size. Furthermore, traditional optimization-oriented state estimation techniques are computationally expensive and are not able to fully monitor the system dynamics and state's variations. Therefore, they may yield to suboptimal solutions. To overcome the mentioned obstacles, a feed-forward back-propagation neural network architecture with one hidden layer is proposed in this paper.

One NN is utilized to monitor the ADN in real-time and evaluate the possibility of congestion. Then another NN will be trained in order to identify the location and cause of the impending line congestion. The inputs of the first NN are active/reactive powers of each bus while the output is the possible line which may face congestion in near future. The output of the first NN, along with the active/reactive power of each bus and their variation are used as the inputs to the second NN. Consequently, the second NN will predict the possible cause of congestion. The general scheme of the proposed intelligent congestion prognosis is presented in Fig. 1. In this figure, z indicates the measurement matrix. Further, $\tilde{x_1}$ and $\tilde{x_2}$ correspond to the estimations of the neural networks.

The training process of the NN involves updating the weights between the neurons and their biases. A loss function is defined as a measure of the quality of the predictions compared to the actual or target values. With each training instant, the goal is to minimize this loss function. The loss function is propagated through the network backwards to fine-tune the weights and biases of each subsequent layer accordingly. This method is known as backpropagation. Several methods, such as Gradient Descent (GD) and Newton's Method (NM) are used for the training purpose. In this paper, a Levenberg-Marquardt (LM) algorithm has been used to iteratively update the weights and biases of the NN [15]. We also incorporate a Bayesian Regularization in excess of the LM algorithm to generalize the trained weights and biases that will lead to a better performance of the NN over the training set.

1) Levenberg-Marquardt algorithm: LM is one of the fastest methods to train a NN, and it leverages the accuracy of Gradient Descent (GD) and the speed of Quasi-Newton method [16]. In this algorithm, the loss function is expressed as a summation of the squared errors as shown in (1):

$$\mathcal{L} = \frac{1}{d}\sum_{i=1}^{d}\left(Y_i - \hat{Y}_i\right)^2 \tag{1}$$

Where, Y_i, $\hat{Y}_i$ and d are the target values, predictions and the number of instances in the dataset respectively. The information regarding the loss function is backpropagated through the layers of the NN, and weights are updated using the approximation of the Hessian matrix as below:

$$w_{ij}^{(k+1)} = w_{ij}^{k} + \mathbf{H}^k g^k \tag{2}$$

Here, the terms w_{ij} denotes the weight matrix between the i^{th} and the j^{th} layers. k is associated with the number of iterations. The terms $\mathbf{H}^k$ and g^k are the 'damped' approximation of the Hessian and the gradient vector respectively.

In LM algorithm, the Jacobian matrix of the loss function with respect to the weight is defined as (3) and used to calculate the approximation of the Hessian matrix as shown in (4):

$$J^k = \frac{\partial \mathcal{L}}{\partial w^k} \tag{3}$$

$$\mathbf{H}^k = [J^{k^T} J^k + \mu I]^{-1} \tag{4}$$

The scalar μ is the damping term which is updated at each iteration. If μ decreases, we would have the Newton's method; while with large value of μ, LM transforms to the GD method. Finally, the gradient g^k is calculated at each step as (5).

$$g^k = J^k \times \mathcal{L} \tag{5}$$

The algorithm terminates when either the gradient or the error falls below a pre-defined threshold or the maximum number of iterations are reached. The same procedure is applied to the biases as well.

2) Bayesian Regularization: In NN training, over-fitting, and over-training are the two common issues which are arisen from the lack of regularization. As a result, the performance of the NN will degrade although the weights and the biases learn the training data accurately. A possible technique to avoid these hurdles is to perform k-fold cross-validation as the whole dataset is divided into 'k' folds. One set is kept for testing and $(k-1)$ folds are used for the NN training. The whole process repeats k times by interchanging the folds between training and testing sets. This process, however, increases the training time [17].

Bayesian regularization method is able to regularize the network without explicitly using a test-set or validation-set. This framework assumes a probability distribution over the entire weight space [18]. The initial space is randomly generated, and then at each step of the iteration, they are updated using the Bayes' rule as below:

$$P(\mathrm{w}|D,\theta) = \frac{P(D|\mathrm{w},\theta)P(\mathrm{w}|\theta)}{P(D|\theta)} \tag{6}$$

Where, D denotes the entire dataset, θ is the performance ratio, $P(D|\mathrm{w},\theta)$ is the likelihood for a given state and the term $P(D|\theta)$ is the normalizer. The main objective of the proposed framework is to maximize the aforementioned probability $P(\mathrm{w}|D,\theta)$, which finds the optimal weight w^*. Maximizing (6) is equivalent to minimizing the loss function in (1). The normalizer in the Gaussian form can be expressed as:

$$P(D|\theta) = g(\theta)Z_F(\theta) \tag{7}$$

$$g(\theta) = \left(\frac{\pi}{\theta}\right)^{-\frac{L}{2}}\left(\frac{\pi}{1-\theta}\right)^{-\frac{L}{2}} \tag{8}$$

$$Z_F(\theta) = \exp\left(-\mathcal{L}(\mathrm{w}^*)\right)\left(det(\mathbf{H})\right)^{-\frac{1}{2}}(2\pi)^{\frac{L}{2}} \tag{9}$$

Therefore, at each iteration of the LM algorithm, after approximating the Hessian matrix by using (6-9) the value w is maximized. The algorithm will be stopped, and w is no longer updated when the optimal w^* is obtained.

III. Simulation and Results

A. Training of the Proposed Neural Networks

Gathering training data for the proposed method is carried out using a modified IEEE standard 13-bus distribution system (Fig. 2) [19]. We made the system balance for this study. Base voltage of 4.16 KV and base power of 4 MVA are considered for this system. Two synchronous generators are added at buses 6 and 13 to derive different test scenarios and impose congestion in multiple lines. Newton Raphson power flow is used to produce a dataset with 546,874 combinations of loads and generations' variations that simulate different operating scenarios. %70 of the dataset is randomly used as a training set, %15 is chosen for the validation set and the remaining %15 is selected as the testing set for the training process.

As mentioned, in the proposed method, the first NN detects the impending congestion in the distribution lines. This NN has ten neurons in the hidden layer, fifteen neurons in the input layer, and twelve neurons in the output layer. The neurons in the input layer are corresponding to the measured system variables (i.e., bus complex voltage V_n , bus active power P_n, bus reactive power Q_n) gathered at time t. We will get the congestion prediction as the output in the form of ones and zeros, where one refers to the high possibility of an imminent congestion. The second NN identifies the cause of the anticipated congestion in order to apply corrective actions to alleviate the problem and avoid further contingencies in the system. For the second NN, forty-two input neurons are considered based on the number of congested lines, loads and generation of each bus, and changes of loads and generations at each sample of the training set. Further, like the previous NN, ten and thirteen neurons are considered in the hidden and output layers respectively. Returning one as the output will recognize the specific buses that cause the congestion.

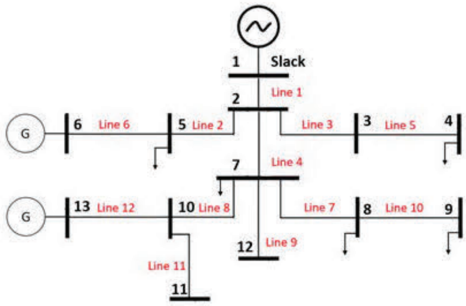

Fig. 2. Modified IEEE 13-Bus Distribution Feeder

As shown in figure 3, the Mean Squared Error (MSE) improves in each training iteration for both NNs. Note that in this figure, the X-axis and the Y-axis are in logarithmic scale.

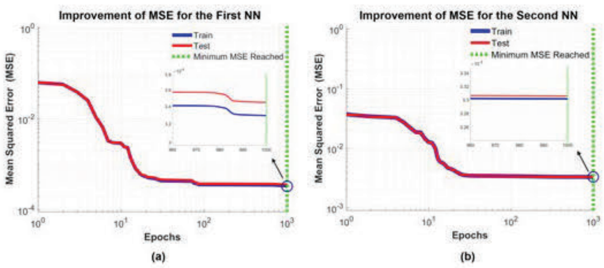

Fig. 3. Improvement of Mean Squared Error for the Neural Networks

B. Performance Evaluation

As our first scenario, we developed a 24-hour load/generation profile based on variable generation at bus 13 to evaluate the performance of the proposed method. The generation of bus 13 is increased linearly from 0 to 4 p.u. and when reached to its maximum, it is decreased linearly to reach 0. Fig. 4 shows the current values for lines 1, 3, and 8. The dashed red line stands for line ampacity; while the blue line represents the currents of the selected lines and the green line shows if a possibility of congestion is detected or not. As seen, line 1 violates the limit from the 12^{th} until the 14^{th} hour and line 8 violates the limit between the 12^{th} and the 14^{th} hour. As shown in the figure, current of line 3 does not violate its limit in this scenario. The green line in Fig. 4 shows that the NNs have successfully predicted the line congestions. For instance, for line 1, the green line changes from zero to one at the 11^{th} hour, indicating that the first NN has predicted a possibility of future congestion and the value stays one until the 15^{th} hour. After the 15^{th} hour, no congestion possibility is detected by the first NN, therefore the green line changes from one to zero.

A second 24-hour scenario is considered where the load of bus 4, is increased linearly from 0 to 1.28 p.u. and when reached its maximum, it is decreased linearly to 0. The NNs' predictions for the two 24-hour scenarios are reported in Table I. The predictions of this table match our expected results. Therefore, the NNs can successfully predict a congestion in a line and its cause in these two scenarios. Based on the estimations from the proposed data-based prognosis method, the operators can take proper control actions. Thus, by utilizing this technique, the possibility of congestion in distribution lines is lowered. Consequently, the distribution system becomes more resilient to sudden changes in loads/generation.

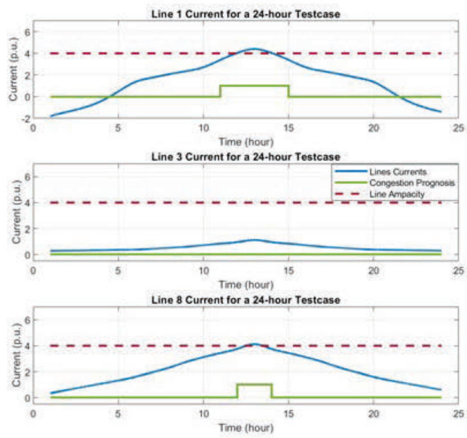

Fig. 4. Selected Line Currents and the Proposed Method Performance for a 24-hour Scenario

Positive predictive values (PPV) and Negative Predictive Values (NPV) are well-known indices for evaluating the accuracy of different approaches in machine learning and statistics. These indices are defined as (10) and (11). True Positives are referring to the cases where there is a congestion and the NN has detected it successfully. Likewise, True Negatives indicate the cases where no congestion is detected by the NN and there

TABLE I
NEURAL NETWORK PREDICTIONS

Scenarios	#1	#2
Congested Lines	1, 8, 12	1, 3, 6
Number of the Bus Causing the Congestion	13	4

was no congestion happening according to the measurement.

$$PPV = \frac{TruePositives}{TruePositives + FalsePositives} \tag{10}$$

$$NPV = \frac{TrueNegatives}{TrueNegatives + FalseNegatives} \tag{11}$$

For further evaluation, the performance of the NNs is tested on two different datasets. The first dataset is the same dataset where the NNs were trained with, whereas the second dataset is generated in a way that only one load or generation change happens in each timestep. Intelligent line congestion prognosis is applied to each of the datasets. In addition, PPV and NPV indices are calculated for each of the datasets, and the results are demonstrated in Table II.

TABLE II
PERFORMANCE OF THE NNS IN DIFFERENT SETS OF DATASETS

PPV

	1^{st} Dataset	2^{nd} Dataset
NN1	99.72%	99.76%
NN2	100%	75.15%

NPV

	1^{st} Dataset	2^{nd} Dataset
NN1	98.85%	98.81%
NN2	54.3%	54.22%

As seen in Table II, both neural networks have an acceptable performance for both of the datasets.

IV. CONCLUSION AND FUTURE WORK

In this paper we trained two neural networks to determine the possible congestion in an ADN and further to detect the possible cause of the congestion. The NNs are trained using a combination of different loads and generations as a training set. Bayesian Regularization alongside with Levenberg-Marquardt algorithm is employed for the training. The performance of the NNs were tested on two datasets. Finally, PPV and NPV indices were introduced to further validate the performance of the NNs in different scenarios. These predictions can be utilized to further improve the power system operation, enabling the operators to foresee possible congestion and act fast to resolve the problem. Hence the resiliency of the ADN is increased and a more reliable operation is guaranteed. Another advantage of the proposed method is that the NNs are trained beforehand, considering the system's specification, hence the detection is in real-time.

In our future work, the NNs will be designed to handle multi-label classifications considering each load-changing bus as a label. Furthermore, evaluation of a time-series predictors such as Long Short Term Memory (LSTM) will be conducted. Finally, the congestion management strategies will be implemented for real-time scenarios, with a focus on energy storage system charge/discharge paradigm and demand response strategies.

REFERENCES

[1] N. I. Yusoff, A. A. M. Zin, and A. B. Khairuddin, "Congestion management in power system: A review," in *2017 3rd International Conference on Power Generation Systems and Renewable Energy Technologies (PGSRET)*, April 2017, pp. 22–27.

[2] "Dispatch of generation and demand side response in regional grids," *2015 IEEE 15th International Conference on Environment and Electrical Engineering, EEEIC 2015 - Conference Proceedings*, pp. 482–486, 2015.

[3] H. Emami and J. A. Sadri, "Congestion Management of Transmission Lines in the Market Environment," *International Research Journal of Applied and Basic Sciences*, vol. 3, pp. 2572–2580, 2012.

[4] J. S. Rao and J. Amarnath, "Transmission Congestion Management Comparative Studies In Restructured Power System," *International Journal of Scientific & Engineering Research*, vol. 4, no. 8, pp. 177–182, 2013.

[5] E. Dehnavi and H. Abdi, "Determining optimal buses for implementing demand response as an effective congestion management method," *IEEE Transactions on Power Systems*, vol. 32, no. 2, pp. 1537–1544, March 2017.

[6] J. Wu, B. Zhang, and Y. Jiang, "Optimal day-ahead demand response contract for congestion management in the deregulated power market considering wind power," *IET Generation, Transmission Distribution*, vol. 12, no. 4, pp. 917–926, 2018.

[7] V. K. Prajapati and V. Mahajan, "Reliability assessment and congestion management of power system with energy storage system and uncertain renewable resources," *Energy*, vol. 215, p. 119134, 2021.

[8] M. A. Fotouhi Ghazvini, G. Lipari, M. Pau, F. Ponci, A. Monti, J. Soares, R. Castro, and Z. Vale, "Congestion management in active distribution networks through demand response implementation," *Sustainable Energy, Grids and Networks*, vol. 17, p. 100185, 2019.

[9] A. Asrari, M. Ansari, and K. C. Bibek, "Real-time congestion prevention in modern distribution power systems via demand response of smart homes," in *2019 North American Power Symposium (NAPS)*, 2019, pp. 1–6.

[10] S. Y. Hadush and L. Meeus, "Dso-tso cooperation issues and solutions for distribution grid congestion management," *Energy Policy*, vol. 120, pp. 610 – 621, 2018.

[11] S. Sharma and L. Srivastava, "Prediction of transmission line overloading using intelligent technique," *Applied Soft Computing*, vol. 8, no. 1, pp. 626 – 633, 2008.

[12] A. M. Glazunova, "Forecasting power system state variables on the basis of dynamic state estimation and artificial neural networks," pp. 470–475, July 2010.

[13] O. Ivanov, M. Gavrilaş, and B. Neagu, "Intelligent monitoring and control in transmission and distribution networks," pp. 185–191, May 2014.

[14] R. Fainti, M. Alamaniotis, and L. H. Tsoukalas, "Three-phase congestion prediction utilizing artificial neural networks," *IISA 2016 - 7th International Conference on Information, Intelligence, Systems and Applications*, pp. 1–5, 2016.

[15] J. J. Moré, "The levenberg-marquardt algorithm: Implementation and theory," in *Numerical Analysis*, G. A. Watson, Ed. Berlin, Heidelberg: Springer Berlin Heidelberg, 1978, pp. 105–116.

[16] J. Nocedal and S. J. Wright, *Numerical Optimization*, 2nd ed. New York, NY, USA: Springer, 2006.

[17] F. Burden and D. Winkler, "Bayesian regularization of neural networks," *Methods in molecular biology (Clifton, N.J.)*, vol. 458, pp. 23–42, 01 2009.

[18] E. Sariev and G. Germano, "Bayesian regularized artificial neural networks for the estimation of the probability of default," *Quantitative Finance*, pp. 1–18, 10 2019.

[19] W. H. Kersting, "Radial distribution test feeders," *IEEE Transactions on Power Systems*, vol. 6, no. 3, pp. 975–985, 1991.

CHAPTER THREE

AGENT-BASED RESILIENT POWER MANAGEMENT OF MICROGRIDS

Abstract

Appropriate planning and optimization strategies for day-ahead power management play important roles in efficient operation of Microgrids (MGs). Due to the uncertainties in electricity demand and renewable generations, and the multi-objective (MO) nature of MG power management, conventional optimization techniques have not been as effective in giving satisfactory results. This chapter aims at solving the day-ahead power management problem as a MO optimization problem, with a focus on increasing the system's resiliency using an agent-based Dynamic Programming (DP) approach named Value Iteration (VI) and a model-free Q-learning (QL) algorithm. The two objectives of the MO problem are: maximizing load serviceability and minimizing operational cost. Both the approaches are data-driven, and the behavior of the agent of each component of a MG is formulated as a finite-horizon Markov Decision Process (MDP). VI guarantees an optimal solution to the MO problem given the MDP model, and QL has the ability to work under uncertainty and incomplete information. The effectiveness of the two algorithms have been evaluated using a benchmark MG test system.

Introduction

Dividing a distribution system into several independent and autonomous entities called Microgrids (MGs) has proven to be a good strategy to deal with the uncertainties of renewable energy resources, electricity demand, and market retail price [1], [2], [3].

Many studies have been conducted to resolve the issue of power management under these uncertainties in MGs. [4] gives an overview of the importance of centralized controllers for stability, power quality, protection and power management of the MG. Stochastic programming is explained in [5] as an approach for power management. Furthermore, in [6], a two-stage stochastic programming was employed to minimize the cost due to the variable nature of renewable energy resources, and in [7], constrained stochastic programming is used to consider the MG limitations. Value Function Approximation is used in [8] to solve a bench marked ESS management problem. Further, in [9], a deep Recurrent Neural Network is used to approximate the value function while considering power flow constraints.

In general, the agent-based power management in a MG on a day-ahead basis can be modeled as a sequential decision-making problem [9], [10]. Under this scheme, the agents controlling the different components of the MG reduce the overall cost while maximizing the utilization of its micro sources for a finite-horizon (e.g., 24 hours), looking at the electricity demand. These utilities include Dispatchable Generators (DGs), Renewable Energy Sources (RESs), Energy Storage Systems (ESSs), and Demand Response (DR) on Price-Sensitive load (PSR). This chapter addresses a MG where the output of the DGs, charging/discharging paradigm of the ESSs, and the PSR can be regulated based on different operating conditions with a primary focus on maximizing the load coverage and a secondary focus on minimizing the cost, using VI and QL, which is in the domain of Reinforcement Learning. Therefore, making the power management problem multiobjective.

Methodology

In this chapter, control of the MG components is formulated as a Markov Decision Process (MDP). We address the load variations and possible duration and intensity of an upcoming extreme event, using its probability of occurrence (assumed to be known from weather forecast) in our simulation. At each discrete time-step (each hour, for example) the output powers for the controllable utilities (DGs, ESSs, DR) are considered as actions, whereas the state-space consists of the supplied electricity demand and the State-of-Charge (SoC) of the ESS. The reward function for each agent is actually a penalty when considering their operating cost or deviation from the target load (the higher the operating cost or deviation from the target load results in higher penalties). The agents interact with the environment to achieve their goal of maximizing their objective functions.

Microgrid Power Management

In general, a MG is connected to the main grid through a Point of Common Coupling (PCC). In our simulation studies, the proposed methods are applied on a modified benchmark MG test system (MG3 from [11]), as shown in Fig. 1. The components of the MG are: a Diesel Generator as DG, several solar photovoltaic (PV) systems, several ESSs (an ESS at each bus with a PV system, not shown in Fig. 1), and some Controllable Loads (CLs). The day-ahead scheduling is performed for a 24-hour horizon with a 1-hour time-step. In this chapter, the power management problem is formulated as a MDP for three agents: a DG agent for the operation and control of the dispatchable generators, a DR agent to perform demand response on the CLs, and an ESS agent to charge/discharge the ESSs. The total PV power is used when available. Therefore, no agent is used for PV generation.

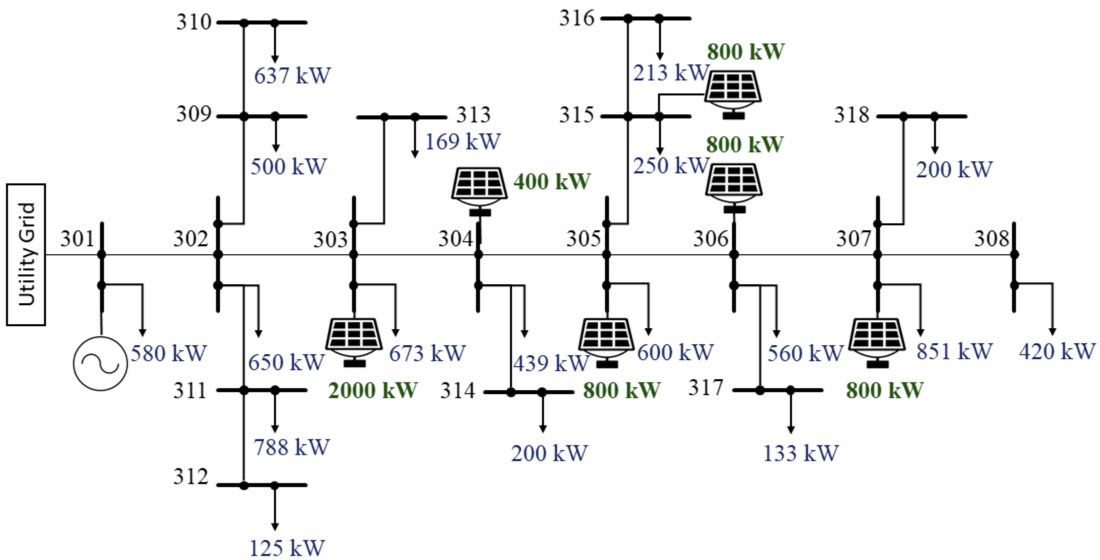

Fig. 1. Single-line diagram of the benchmark MG system.

<u>Formulation of MDP</u>

A finite-horizon MDP can be defined as a 5-tuple $M =< S, A, R, T, H >$ where, S is a finite set of state variables, A is a finite set of actions, R is the immediate reward observed after reaching a state, $s \in S$. T is the set of transition probabilities for the transition of one state to another with a specific action [12], and H is the length of the horizon. For simplicity of implementation for both Value Iteration (VI) and Q-learning (QL) algorithms, the state-action space is discretized to their nearest integers. For the implementation of VI algorithm in our power application, the transition probability of reaching a particular state S_j using an action a_{ij} from state si is assumed to be 1, s_i,

$s_j \in S$, $a_{ij} \in A$ [13]. The detailed models of the associated agents are described in the rest of this section.

<u>DG Agent</u> The DG agent is responsible for setting the output of the DG located in the MG, as per the electricity demand. In a MG, if P_t^{DG} is the active power output of the DG at a time step t, then for each DG, the operational constraints are as follows:

$$P_{DG}^{min} \leq P_{DG}^{t} \leq P_{DG}^{max} \tag{1}$$

$$|P_{DG}^{t} - P_{DG}^{t-1}| \leq \rho \times \Delta t \tag{2}$$

Here, the max and min terms represent the maximum and minimum output of the generator [9]. The term ρ represents the limit of the increase/decrease of generation at each time step and is known as the Generation Rate Constant (GRC).

For the DG agent, the set of states consists of the pos-sible load coverage by the DG, and is defined by $S_{DG} = \left\{ s_{DG_j}^{t} \middle| \forall j \in S_{DG}, P_{DG}^{min} \leq s_{DG_j}^{t} \leq P_{DG}^{max} \right\}$. Only the active power outputs have been considered in this work. The action set is the range of feasible discrete set-points of the generator outputs, defined as: $A_{DG} = \{a_{DG_i}^{t} \mid \forall i \in A_{DG}, |a_{DG_i}^{t}| \leq \rho \times \Delta t\}$

Each DG has an operational cost, which is a function of the active power output of the DG. For this chapter, a quadratic cost function is considered, as defined in [14]. The cost function denotes that the higher output power results in higher cost, which is a penalty, denoted by a negative sign. At the same time, the DG focuses on maximum coverage of load. Therefore, the reward function for the DG agent is defined as follows:

$$R_{DG}(s_{DG_j}^{t}, a_{DG_i}^{t}) = -\frac{\{\overset{\text{Generation Cost}}{\boxed{\left(\alpha + \beta(P_{DG}^{t}) + \gamma(P_{DG}^{t})^2\right)}} - \overset{\text{Retail Price}}{\boxed{(\lambda^t P_{DG}^{t})}}\}}{N_1} w_1 - \frac{(\overset{\text{Electricity Demand}}{\boxed{P_L^t}} - P_{DG}^{t})}{N_2} w_2 \tag{3}$$

where, α, β and γ are the generation cost coefficients [14], P_L^t and P_{PV}^t are the predictions of electricity demand and PV output, λ^t is the market electricity price forecast at time step t. w1 and w2 are the weight factors, and N_1 and N_2 are the normalization factors, respectively [15]. Here, it should be noted that during an extreme event resulting in grid blackout, which islands the MG, the term λ^t is zero.

DR Agent The task of the DR agent is to perform PSR on CLs. In case of insufficient generation, a percentage of the electricity demand is available for curtailment (the maximum percentage is given in Table I), associated with a penalty for causing discomfort to the user. The total electricity demand for the time horizon H is denoted $by\ P_L = \{P_L^t, \forall t = 1, 2, 3, \ldots H\}$. For the DR agent, only the active power is considered.

The state space for the DR agent is the permissible range of the curtailed loads $S_{DR} = \left\{s_{DR_j}^t \middle| \forall j \in S_{DR}, P_L^{t^{min}} \leq s_{DR_j}^t \leq P_L^{t^{max}}\right\}$. The action space for the DR agent is defined as $A_{DR} = \{a_{DR_i}^t \mid \forall i \in A_{DR}, |a_{DR_i}^t| \leq P_{DR}^{t^{max}}\}$. A_{DR} is restricted by the range of deviations of set-points, $P\ tDR = P_L^t - P_{sup}^t$ The load-shedding penalty for the DR is expressed as the following piece-wise linear model [9]:

$$P_{CL}^t = \begin{cases} \delta_0(P_L^t - P_{sup}^t) + \phi_0, & P_{L_{max}}^t \geq P_{sup}^t \geq P_{L_1}^t \\ \delta_1(P_L^t - P_{sup}^t) + \phi_1, & P_{L_1}^t \geq P_{sup}^t \geq P_{L_2}^t \\ \delta_2(P_L^t - P_{sup}^t) + \phi_2, & P_{L_2}^t \geq P_{sup}^t \geq P_{L_{min}}^t \end{cases} \tag{4}$$

Here, $\delta_0, \delta_1, \delta_2, \varphi_0, \varphi_1,$ and φ_2 are the constant coefficients for the load-shedding penalty model. P_{sup}^t is the amount of load that is not curtailed, and hence to be supplied. Both P_{L1}^t and P_{L2}^t are set points representing the mild, and moderate curtailment levels, as described in [16]. However, at the same time, the DR agent should consider the cost of supplying the loads, as per market electricity price. Therefore, the overall reward function for the DR agent becomes:

$$R_{DR}(s^t_{DR_j}, a^t_{DR_i}) = -\frac{P^t_{CL}}{N_3} w_3 - \frac{\lambda^t (P^t_L - P^t_{PV})}{N_4} w_4. \quad (5)$$

Here, ω_3 and ω_4 are the weight factors, and N_3 and N_4 are the normalization factors, respectively [17].

ESS Agent The ESS agent is responsible for maximum load coverage during an extreme event, when the generation units are out of service. The agent considers the extreme event forecast at each hour of the next day, starts storing energy to supply the highest possible loads during the extreme event. Prior to the extreme event, additional energy will charge the ESS. For controlling the amount of energy stored in the ESS, the State of Charge (SoC) of the battery at each time step is defined as follows:

$$SoC^t_{ESS} = \frac{E^t}{E_{Cap}} \quad (6)$$

where E_t is the amount of energy stored in the ESS at time step t, and E_{Cap} is the energy capacity of the storage unit.

Typically, ESS should not be fully discharged; otherwise the storage unit might be seriously damaged. The limits for SoC which is known as capacity constraint of the ESS is shown below:

$$SoC^{min}_{ESS} \leq SoC^t_{ESS} \leq SoC^{max}_{ESS} \quad (7)$$

where SoC_{min} and SoC_{max} respectively denote the minimum and maximum allowed SoC at each time step. Also, E_{max} and E_{min} indicate the maximum and minimum allowed stored energy. Looking at Eq. 7 the state space for the ESS agent can be represented as $S_{ESS} = \{s^t_{ESS_j} \mid \forall j \in S_{ESS}, SoC^{min}_{ESS} \leq s^t_{ESS_j} \leq SoC^{max}_{ESS}\}$ The charging and discharging rates of the ESS (P_{ESS}) are considered as actions for the ESS agent. Accordingly, the action space for this agent is described as $A_{ESS} = \{a^t_{ESS_j} \mid \forall i \in A_{ESS}, |a^t_{ESS_i}| \leq P^{max}_{ESS}\}$.

The reward function of the ESS agent is:

$$R_{ESS}(s^t_{ESS_j}, a^t_{ESS_i}) = \begin{cases} SoC^{max}_{BESS} - SoC^t_{BESS} & \mu^t > 0.1 \,\&\, \mu^t \neq 1 \\ SoC^t_{BESS} \times E_{Cap} - P^t_L & (\mu^t = 1 \; Or \; M = 1) \\ SoC^t_{BESS} - SoC^{min}_{BESS} & else \end{cases} \tag{8}$$

where μ^t represents the probability of the extreme event at time step t. M is a flag indicating whether the grid is still under maintenance, or it is healthy. When healthy, the MG can be reconnected to the grid.

<u>Power Management in a MDP Framework</u> The agent-based scheduling for a MG is formulated as an optimization problem under a MDP framework with the following set of objective function:

$$\max_{a_{DG}, a_{DR}, a_{ESS}} \sum_{t=1}^{H} \{R_{DG}, R_{DR}, R_{ESS}\} \tag{9}$$

subject to (1), (2), (4),(6),(7).

Solution Approached for MDP To solve the above-mentioned MDP problem, the Value Iteration (VI) algorithm is applied [18]. In this DP method, the optimal value of a state is calculated with the help of the following equation [19]:

$$Q(s_t, a_t) := E[r|s_t, a_t] + \Gamma \sum_{s'_t \in \mathcal{S}} P(s'_t|s_t, a_t)V(s'_t) \qquad (10)$$

where, $E[r|s_t, a_t]$ denotes the expected immediate reward. The probability of transition from state s_t to s'_t by taking an action at, is represented by $P\ (s'_t|s_t, a_t)$. Γ is the discount factor, which determines the impact of the future rewards for a specific state. The values are said to converge when the difference between the values obtained from two consecutive iterations are less than a pre-defined threshold, θ.

$$V(s_t) = \max_{a \in \mathcal{A}} Q(s_t, a_t) \qquad (11)$$

$$\max_{s \in \mathcal{S}} |V(s_t)^k - V(s_t)^{k+1}| < \theta \qquad (12)$$

The MDP has also been solved using a temporal difference algorithm, namely Q-learning (QL). This algorithm learns the best action to move from one state to another based on the maximum expected values of the reward functions, without knowing the transition probability. The transition probability is used in the case of VI, but not in the case of QL. The experience gathered by each agent from the interaction with the state-space is recorded in a look-up-table, named Q-table. Using a specific state-action pair, the agents interact with the environment and the corresponding Q-table values are updated by a running average mechanism [20], [21].

Numerical Experiments and Results

Test Case

The proposed method is validated on the benchmark test MG system as a grid-connected MG (MG3 from [11]), as shown in Fig. 1. A 24-hour time horizon is considered for the whole simulation with a 1-hour window time-step. In our simulation, an extreme event occurs at hour 12 when both the grid and the DG go out of service. The extreme event continues until hour 14, after which a maintenance phase starts for the grid and the DG until hour 21, as shown in Fig. 6. The probability of occurrence of an extreme event at each time step is also shown in the figure. Note that, the probability keeps increasing before hour 12 and starts decreasing when the extreme event is over at hour 14. The forecasted electricity demand, PV output data, and system specification is adopted from [11]. The retail electricity price data were obtained from [17]. The technical information about the components of the MG is displayed in Table 1.

Table 1- Power/Energy Capacity of The Components of The Test System

Components	**Max. Capacity (MW)**	**Min. Capacity (MW)**
DG	7	2.5
PV	5.6	0
P_L^t	7.988	6.63
CL	40% of P_L^t	0% of P_L^t
ESS	28.6 (MWh)	4.967 (MWh)

For the DG agent, the GRC constant, ρ, the generator cost coefficients α, β and γ were selected as 700 kW, \$14.67, \$0.1709/kWh, and \$0.0001773/(kWh)2, respectively. For the DR agent, the constant coefficients $\delta 0$, $\delta 1$ and $\delta 2$ were set as 0.3, 0.5 and 0.75, respectively. All the φ values were set to 0.

The curtailment levels, PL_1^t and PL_2^twere selected as 90%and 30% of the permissible range, SDR, respectively. The weight factors for the reward functions were set as, ω_1 = 0.7, ω_2= 0.3, ω_3= 0.7 and ω_4= 0.5, to ensure that the main objective of the agents is maximizing load coverage rather than minimizing cost.

For VI, Γ and θ were chosen to be 0.99 and 0.001, respectively. For QL, the learning rate η is selected to be 0.1. The $\epsilon - greedy$ algorithm has been used for the QL action selection [19], and the value of ϵ (exploration rate) was initially chosen as 0.9 for every state-action pair in the Q-table with a decay rate of 0.95 for each visit of the agent.

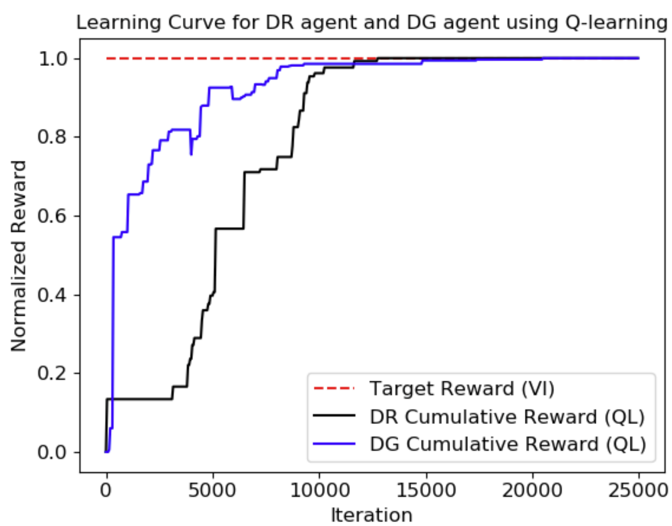

Fig. 2. Cumulative reward of the 24-hour planning horizon for the DG agent and the DR agent at each iteration using QL algorithm.

Agent-based Power Management

The DG agent and the DR agent were trained to find a strategy for the DG, and the supplied load based on the retail price and customer discomfort level, respectively. Whereas, the ESS agent learns a strategy to prepare and provide energy to the MG to cover the essential loads (when possible) in case of a grid blackout due to a fault or an extreme event. During this period, the MG is islanded, and the DG is assumed to be out of service. Therefore, PV and ESS will cover the essential loads (assumed to be 50% of the total load). Fig. 2 shows the learning curve of the DG agent and DR agent for QL with respect to the number of iterations

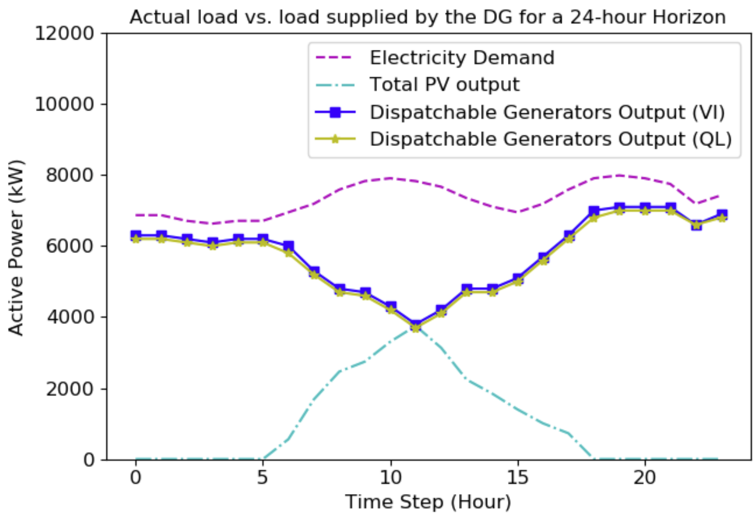

Fig. 3. Economic Dispatch of the DG agent using VI and QL.

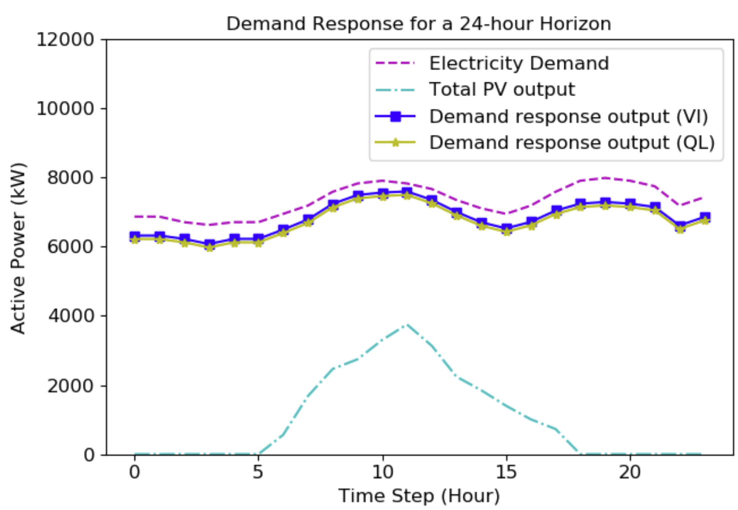

Fig. 4. Day-ahead scheduling of the DR agent using VI and QL.

The reward obtained through value-iteration is considered to be the target reward. From Fig. 2, the DR agent reaches the target value in about 12000 iterations and the DG agent in about 19000 iterations.

The selected states by the DG agent and the DR agent using both VI and QL are shown in Figs. 3 and 4, respectively along with the forecasted electricity demand and the renewable generation (PV). The policy that sequentially transits from one optimal state to another is considered to be the optimal policy. The learned optimal policy for the ESS is demonstrated in Fig. 5. As shown in the figure, from t = 3 (when the extreme event probability is more than 10%) the battery starts storing as much energy as it can (SoC_{ESS}^{max}) (Fig. 6) so that it can cover maximum loads possible during the extreme event. After the recovery time, the normal operation of the MG is continued.

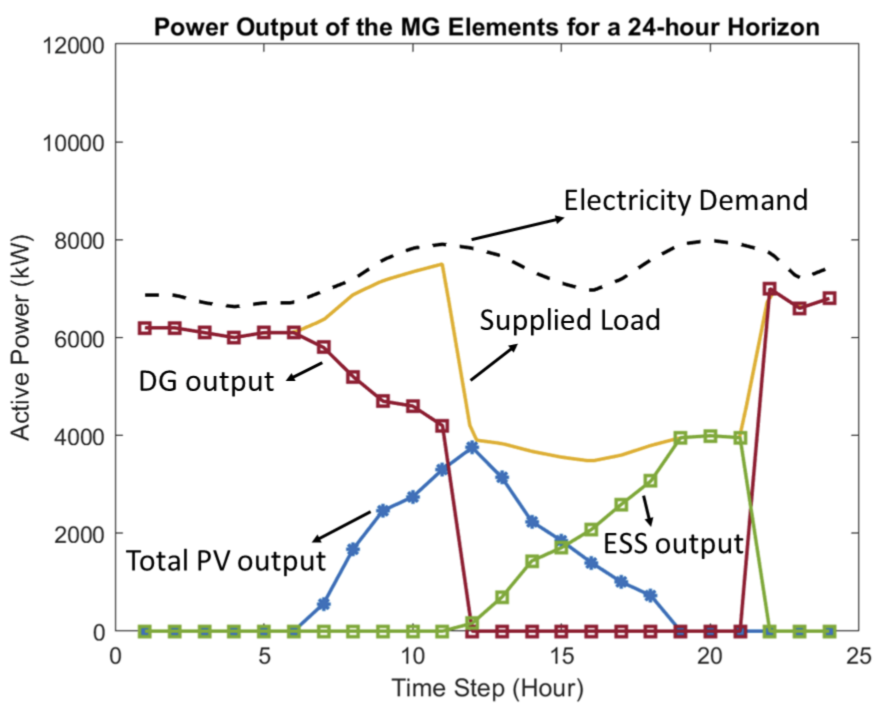

Fig. 5. Load coverage of the ESS agent under an extreme event scenario.

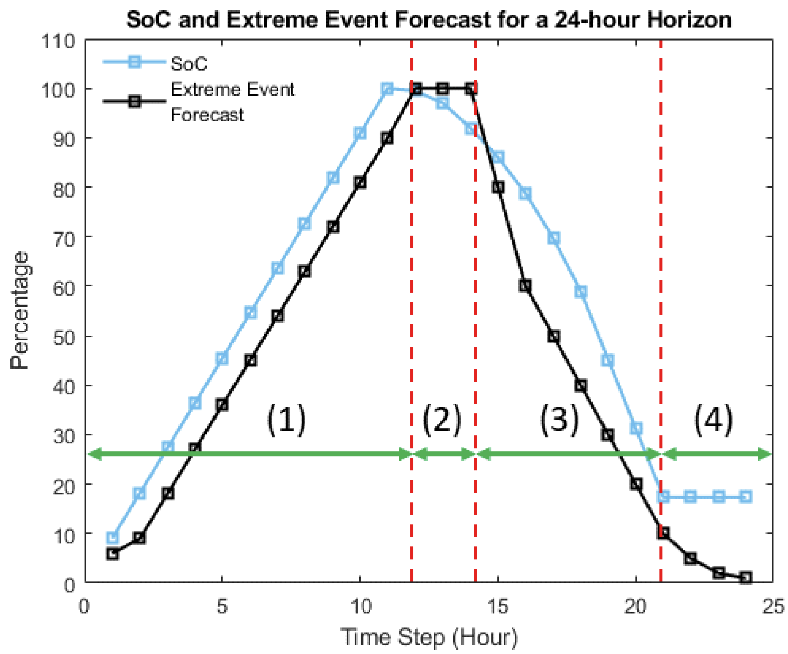

Fig. 6. Percentage of State of Charge (SOC) of the ESS for the 24-hour horizon, along with the probability of occurrence of an extreme event: (1) pre-extreme event, (2) during extreme event, (3) maintenance period, and (4) normal operation.

Discussion

As mentioned in section II, the reward function for each agent has two inversely proportional components of different weights. Considering that the main focus of the agents is maximum load coverage, Figs. 3 and 4 show that using both the VI and QL algorithms, the agents learn to operate in between the feasible state spaces and take proper actions. For the DG agent, when the load change is more than the GRC constant (2), the change of generation is bound by the GRC. On the other hand, the DR agent is mostly operating within (80-100)% of the actual electricity demand at each hour. Finally, the performance of the system was examined in the presence of an ESS agent, in a scenario where there was a possibility of an extreme event. As shown in Fig. 5, before hour 6, 90% of the load is supplied by the generator. From hour 6 to 11, the combination of the generator and PV supplies the load. However, during the extreme event, since the generator is out of service, the combination of the PV and ESS covers the essential load (50% of the total load). After the recovery time, the MG resumes its normal operation.

Conclusions and Future Work

This formulates the power management of a MG as a MDP, and solves the sequential decision-making problem using two algorithms: VI and QL. The three agents, controlling the DG, CLs, and the ESS have been trained to find the solution to the proposed multiobjective problem, with the pri-mary focus on maximizing the load coverage and a secondary focus on minimizing the operation cost for a day-ahead finite-horizon.

In case of loss of generation due to an extreme event, the agents would cooperate to make the MG survive with partial load coverage, thus enhancing the resiliency of the system.

References

[1] A. Chaouachi, R. Kamel, R. Andoulsi, and K. Nagasaka, “Multiobjective intelligent energy management for a microgrid,” IEEE Trans. Indust. Elec., vol. 60, pp. 1688–1699, Apr. 2013.

[2] R. Lasseter, “Microgrids,” Proc. IEEE Power Eng. Society Trans. and Dist. Conf., vol. 1, pp. 305 – 308, Jan. 2002.

[3] C. Schwaegerl, “Advanced architectures and control concepts for more microgrids,” More Microgrids, Siemens AG, STREP, no. 1, pp. 1–145, 2009.

[4] A. Kaur, J. Kaushal, and P. Basak, “A review on microgrid central controller,” Renew. Sustain. Energy Rev., vol. 55, pp. 338–345, 2016.

[5] W. Su, J. Wang, and J. Roh, “Stochastic energy scheduling in microgrids with intermittent renewable energy resources,” IEEE Trans. Smart Grid, vol. 5, pp. 13–27, 2013.

[6] T. Nguyen and M. Crow, “Stochastic optimization of renewable-based microgrid operation incorporating battery operating cost,” IEEE Trans. Power Syst., vol. 31, pp. 2289 – 2296, 2015.

[7] Y. Zhang, N. Gatsis, and G. Giannakis, “Robust energy management for microgrids with high-penetration renewables,” IEEE Trans. Sustain. Energy, vol. 4, 2012.

[8] D. Jiang, T. Pham, W. Powell, D. Salas, and W. Scott, “A comparison of approximate dynamic programming techniques on benchmark energy storage problems: Does anything work?” 2014 IEEE Symposium on Adaptive Dynamic Programming and Reinforcement Learning (ADPRL), pp. 1–8, 2014.

[9] P. Zeng, H. Li, H. He, and S. Li, “Dynamic energy management of a microgrid using approximate dynamic programming and deep recurrent neural network learning,” IEEE Trans. Smart Grid, vol. PP, pp. 171–188, 2018.

[10] S. Zhou, Z. Hu, W. Gu, M. Jiang, and X.-P. Zhang, “Artificial intel-ligence based smart energy community management: A reinforcement learning approach,” CSEE J. Power Energy Syst., vol. 5, 03 2019.

[11] M. N. Alam, S. Chakrabarti, and X. Liang, “A benchmark test system for networked microgrids,” IEEE Trans. Ind. Informat., vol. 16, no. 10, pp. 6217–6230, 2020.

[12] A. G. Barto, S. J. Bradtke, and S. P. Singh, “Learning to act using real-time dynamic programming,” Artif. Intell., vol. 72, no. 1–2, 1995.

[13] C. Essayeh, M. Raiss El-Fenni, and H. Dahmouni, "Towards an intelli-gent home energy management system for smart microgrid applications," 2016 International Wireless Communications and Mobile Computing Conference (IWCMC), pp. 1051–1056, 2016.

[14] S. A. Pourmousavi Kani, M. H. Nehrir, and R. Sharma, "Multi-timescale power management for islanded microgrids including storage and demand response," IEEE Trans. Smart Grid, vol. 6, pp. 1185–1195, 2015.

[15] K. Dehghanpour and H. Nehrir, "A market-based resilient power man-agement technique for distribution systems with multiple microgrids using a multi-agent system approach," Electric Power Comp. Syst., vol. 46, no. 16-17, pp. 1744–1755, 2018.

[16] B. Moran, "Microgrid load management and control strategies," IEEE/PES Transmission and Distribution Conference and Exposition (T&D), pp. 1–4, 2016.

[17] K. Dehghanpour, M. H. Nehrir, J. W. Sheppard, and N. C. Kelly, "Agent-based modeling of retail electrical energy markets with demand response," IEEE Trans. Smart Grid, vol. 9, no. 4, pp. 3465–3475, 2018.

[18] R. Bellman, "A markovian decision process," Journal of Mathematics and Mechanics, vol. 6, no. 5, pp. 679–684, 1957.

[19] E. Alpaydin, Introduction to Machine Learning, 3rd ed. MIT Press, 2014.

[20] C. J. C. H. Watkins, "Learning from delayed rewards," Ph.D. disserta-tion, King's College, Cambridge, UK, 1989.

[21] C. J. Watkins and P. Dayan, "Q-learning," Machine learning, vol. 8, no. 3-4, pp. 279–292, 1992.

CHAPTER FOUR

RESILIENCY-ORIENTED OPTIMIZATION OF CRITICAL PARAMETERS IN MULTI INVERTER-FED DISTRIBUTED GENERATION SYSTEMS

Contribution of Authors and Co-Authors

Manuscript in Chapter Four

Author: Mohammad Alali

Contributions: Suggested the main idea, prepared the manuscript, simulated the problem and coded the optimization part, analyzed the obtained results from the simulation.

Co-Author: Dr. Zagros Shahooei

Contributions: Provided important insight and overview of the problem, interpretation of results, and aided in the preparation and editing of the manuscript and figures.

Co-Author: Dr. Maryam Bahramipanah

Contributions: Provided important insight and overview of the problem, interpretation of results, and aided in the preparation and editing of the manuscript and figures.

Manuscript Information

Mohammad Alali, Zagros Shahooei, Maryam Bahramipanah

Sustainability Journal: Special Issue "Optimal Dynamic Control of Active Distribution Power System"

Status of Manuscript:
_X_ Prepared for submission to a peer-reviewed journal
____ Officially submitted to a peer-reviewed journal
____ Accepted by a peer-reviewed journal
____ Published in a peer-reviewed journal

Publisher: MDPI

sustainability

MDPI

Article

Resiliency-Oriented Optimization of Critical Parameters in Multi Inverter-Fed Distributed Generation Systems

Mohammad Alali [1]*, Zagros Shahooei [1], and Maryam Bahramipanah [1]

[1] Montana State University; MohammadAlali@montana.edu; Zagros.shahooei@montana.edu Maryam.bahramipanah@montana.edu
* MohammadAlali@montana.edu

Abstract: In the modern power grid, with the growing penetration of renewable and distributed energy systems, the use of parallel inverters has significantly increased. It is essential to achieve stable parallel operation and reasonable power sharing between these parallel inverters. Droop controllers are commonly used to control the power sharing between parallel inverters in an inverter-based microgrid. In this paper, a small signal model of a droop controller with secondary loop control and an internal model-based voltage and current controller is proposed to improve the stability and power sharing of inverter-based Distributed Generation (DG) systems. The DG system's nonlinear dynamic equations are derived by incorporating the appropriate and accurate models of the network, load, PLL and filters. The obtained model is then trimmed and linearized around its operating point to find the DG system's state space representation. Moreover, we optimize the critical control parameters of the model, which are found using eigenvalue analysis, using Grey Wolf Optimization technique. Through time-domain simulations, we show that our proposed method improves the system's resiliency, stability, and power sharing characteristics.

Keywords: Controller Optimization; Droop Control; Grey Wolf Optimizer; Internal Model Control; Inverter; Microgrid; Resiliency; Secondary Control Loop; Small-Signal Stability

Citation: Lastname, F.; Lastname, F.; Lastname, F. Title. *Sustainability* **2021**, *13*, x. https://doi.org/10.3390/xxxxx

Academic Editor: Firstname Lastname

Received: date
Accepted: date
Published: date

Nomenclature

$\boldsymbol{Z}$	Impedance of the transmission line between the DGs
$\boldsymbol{i},\boldsymbol{j}$	Index of nodes
$\boldsymbol{V_i}$	Voltage of $\boldsymbol{DG_i}$
$\boldsymbol{\delta_i}$	Phase of $\boldsymbol{DG_i}$
$\boldsymbol{P}$	Real power of the inverter
$\boldsymbol{Q}$	Reactive power of the inverter
$\boldsymbol{\widetilde{P}}$	Instantaneous real power of the inverter
$\boldsymbol{\widetilde{Q}}$	Instantaneous reactive power of the inverter
$\boldsymbol{P_{ir}}$	Real power reference for inverter i
$\boldsymbol{Q_{ir}}$	Reactive power reference for inverter i
$\boldsymbol{\omega_c}$	Value of fitness function
$\boldsymbol{V_{i,abc}}$	Voltage of node i in $\boldsymbol{abc}$ reference frame
$\boldsymbol{V_{i,dq}}$	Voltage of node i in $\boldsymbol{dq}$ reference frame
$\boldsymbol{i_{j,abc}}$	Current of node j in $\boldsymbol{abc}$ reference frame
$\boldsymbol{i_{j,abc}}$	Current of node j in $\boldsymbol{dq}$ reference frame

$\boldsymbol{V}^*$	Output voltage of the power controller Used as a reference voltage for the IMC voltage controller
$\boldsymbol{\omega}^*$	Output frequency of the power controller Used as a reference frequency for the IMC voltage controller
$\boldsymbol{\omega_{pll}}$	Angular frequency of the PLL
$\boldsymbol{\omega_n}$	Reference angular frequency
$\boldsymbol{V_n}$	Reference voltage
$\boldsymbol{\omega_i}$	Angular frequency of the inverters
$\boldsymbol{L_i}$	Inductors used in the lowpass filter
$\boldsymbol{r_i}$	Resistors used in the lowpass filter
$\boldsymbol{R_d}$	Used to model the capacitor's series resistance
$\boldsymbol{C_f}$	Capacitor of the lowpass filter
$\boldsymbol{K_{pv}}$	The coefficient for the proportional controller related to the voltage controller
$\boldsymbol{K_{iv}}$	The coefficient for the integral controller related to the voltage controller
$\boldsymbol{K_{dv}}$	The coefficient for the derivative controller related to the voltage controller
$\boldsymbol{K_{pc}}$	The coefficient for the proportional controller related to the current controller
$\boldsymbol{K_{ic}}$	The coefficient for the integral controller related to the current controller
$\boldsymbol{K_{dc}}$	The coefficient for the derivative controller related to the current controller
$\boldsymbol{K_{pd}(s)}$	Transfer function of the PD controller in the internal model-based controller
$\boldsymbol{K_{pi}(s)}$	Transfer function of the PI controller in the internal model-based controller
$\boldsymbol{K_{pid}(s)}$	Transfer function of the PID controller in the internal model-based controller
$\boldsymbol{\lambda_v}$	Tuning parameter for the IMC voltage controller
$\boldsymbol{\lambda_c}$	Tuning parameter for the IMC current controller
$\boldsymbol{T_c}$	Time period of the inverter output signal
$\boldsymbol{T_{pwm}}$	Time period of the inverter switching
$\boldsymbol{\phi_i}$	States of the IMC voltage controller
$\boldsymbol{\gamma_i}$	States of the IMC current controller
$\boldsymbol{V_{bDi}}$	Input voltage in d-axis
$\boldsymbol{V_{bQi}}$	Input voltage in q-axis
$\boldsymbol{R_N}$	Virtual resistor
$\boldsymbol{m}$	One of the Control parameters of the power controller used to control the voltage

1. Introduction

With increasing penetration of distributed renewable energy resources in power system, grid's stability and operation is becoming more important. Due to the distributed characteristic of these generations, Micro-Grids (MGs) are formed as decentralized groups of generation units and loads. MGs may work in grid-connected or islanded configurations to provide efficient, resilient, reliable, and clean energy [1-2]. Unlike traditional utility grids, which have large synchronous generators, MGs generally consist of low inertia renewable and distributed generation systems. Therefore, they are more prone to instability due to contingencies or extreme events. Consequently, operation and control issues are extremely important, especially in an islanded mode.

The DG's inverters are mostly connected in parallel to the grid to improve power sharing and stable performances [3]. Hence, designing a robust controller for Inverter-based Distributed Generations (IDGs) plays a critical role to improve the stability and resiliency of MGs.

Sensitivity and eigenvalue analysis are two common methods used along with the Small Signal Stability (SSS) analysis to improve the stability and resiliency of the MGs. One benefit of the SSS is that it is highly dependent on the accuracy of the mathematical models of the devices in the MG. Different DG systems are discussed in [4] and different types of the inverters are described based on the frequency regions. Also, it is shown that the power controller coefficients are within the low frequency region, which is generally known as the dominant mode. [5] presents a SSS study to optimize the parameters of the inverter's PI current controller using Particles Swarm Optimization (PSO); however, in [5], the SSS analysis was only performed on the PI controller and mathematical model of the other components is not considered. [6] utilizes PSO to directly tune the control parameters without any SSS analysis. This can significantly increase the computation burden since there are no constraints for the parameters during the optimization process. In [7], the problems with [5] and [6] has been addressed and all the MGs' controllers are optimized after identifying the significant control parameters using SSS.

Droop control is one of the most common approaches introduced for improving MGs' stability, resiliency, and power sharing between parallel inverters. In [8] a virtual flux droop is used to achieve voltage and frequency stability and equal power sharing. [9] proposes a modified droop controller to improve the transient response and stability margins. Droop coefficients have a direct effect on the SSS analysis. It is shown that large droop coefficients deteriorate the stability and resiliency which can lead to high power output in some of the sources that can cause failures and even blackouts. On the other hand, small droop coefficients can result in unequal power sharing. Network parameters play an important role in power sharing. A very small mismatch between different DG's network parameters would lead to large differences in the shared power between the inverters. Therefore, sensitivity analysis is often used to determine the droop coefficients to improve the stability, resiliency, and power sharing of the IDGs [10-16].

In [17-20], SSS analysis is investigated under different load conditions. Further, in [4], [10], [12-14], [17-20], small signal analysis is studied in a system which uses PI controller to control the voltage and current in the dq axes. However, the dq axes are not fully decoupled and variations of one of the axes might lead to transients on the other one. To have a more stable dynamic performance, Internal Model Control (IMC) is used in IDGs using the state space [21]; while in [3] the developed model is validated using SSS analysis. The results from [21] and [22] show that IMC significantly improvs the stability of the IDGs in comparison to conventional PI voltage and current controllers. Nonetheless, in the previously mentioned literature, the models of the filter and the Phase Locked Loop (PLL) are not considered in the stability analysis. [23] presents a SSS analysis, considering the filter and PLL models and using a PI controller. However, oscillatory modes are neglected in [23] due to the large amount of the damping resistor.

Further, SSS analysis of IDGs using conventional droop controller is investigated in [9-11], [14-23]. Although the conventional droop controller is generally incorporated to increase the reliability and resiliency of the system, it has two major drawbacks. The first problem is voltage and frequency changes due to a sudden load variation. The second limitation is improper load sharing when the output impedances of the inverters don't match. To solve these issues, a robust controller and a universal droop controller are suggested in [24] and [3], respectively. Furthermore, [25] shows a SSS analysis for the universal droop controller. However, it does not investigate the effects of the critical control parameters on the stability and resiliency of the system. Authors in [26] develop a droop controller with secondary control loop to achieve equal power sharing between parallel inverters regardless of the output impedances of the inverters. However, the effects of the filter elements, PLL and network and load models are not considered.

In the past decade, the resiliency of modern power system has gained a lot of attention. Resiliency is defined as the ability of the power system to withstand extreme events and recover rapidly with the minimum damage. [33] investigates the effects of power-electronic interfaces, energy storage systems (ESSs) and distribution system architectures on the resiliency of MGs and improves the resiliency during extreme events. [34] proposes an advanced control strategy for power electronic converters and suggests an energy management scheme for MGs with photovoltaic and battery ESSs. It uses model predictive control strategy to minimize the operating cost, maximize the profit and obtain energy resiliency of the MG system. Furthermore, [35] proposes a two-stage, coordinated power sharing strategy between battery ESSs and coupled MGs for overload management in MGs, using dynamic frequency control. In this study we aim to maintain stability by fast restoration and reduce the impacts of different disturbances in order to improve the resiliency of the DG System.

Heuristic algorithms have received a lot of attention in the recent years due to their high speed and efficiency in solving optimization problems. One of the promising heuristic methods especially in the power system and power electronic applications, is Grey Wolf Optimizer (GWO) [10]. In [28], a chaotic GWO is proposed to minimize the power losses and improve the voltage stability in order to size and site DGs in the system. Also, the chaotic GWO determines the optimal droop parameters. [29] uses GWO to optimize the control parameters of the proportional resonant controllers and find the optimal design of the output filter of a grid-tied inverter. Furthermore, Djerioui et al. in [30] present a predictive torque control of a permanent magnet synchronous motor based on GWO for smooth operation of electric vehicles. Specifically, the authors try to minimize the oscillations at low-speed operation of the motor. In [31], the optimal allocation of DGs is investigated to minimize the power losses while meeting the real and reactive demands in a distribution network. Also, [32] proposes an optimization problem to minimize the total cost of the two-terminal HVDC system by incorporating the GWO in the optimal power flow algorithm. In this paper, we propose a novel methodology to improve the stability, resiliency, and power sharing of IDGs using GWO algorithm. The contributions of this paper are as follows:

- Detailed mathematical modeling and equations of an IDG containing droop control with secondary control loop and an IMC-based voltage and current controller is presented.
- The state space equations of the system are derived by linearization using Linear Analysis Tool in MATLAB/SIMULINK. The system matrix is then introduced.
- Critical control parameters of the system are identified after the eigenvalue and sensitivity analysis on the system matrix. After finding the stability domains of the critical parameters, GWO is used to find the optimal critical parameters for the controllers.

- The DG system's stability and power sharing characteristics are verified in time domain simulations by applying different load disturbances at different time steps.
- Finally, it is shown that the resiliency of the DG system is significantly improved by comparing different stability indices.

The remainder of this paper is organized as follows. Section 2 provides a detailed description of the mathematical modeling and equations of the MG components. In section 3, the linearization and state space equations of the MG system is discussed in detail. In section 4, eigenvalue, and sensitivity analysis of the MG system are investigated. Furthermore, critical control parameters of each component are recognized, and the parameter stability domains are presented. After which, the optimal control parameters are derived using GWO. Section 5 presents the simulation results and performance evaluation of the optimal parameters. Finally, conclusions and discussions of the future work are presented in section 6.

2. Mathematical Modeling

In this work, we consider a microgrid with two DGs connected through a power line with impedance Z. The system is shown in Figure 1(a). Each DG is connected to a static load. Figure 1(b) shows the DGs' system block diagram including the LCL filter, voltage and current controller, PLL and power controller. The mathematical modelling of each component along with the dynamics of the loads and the network are discussed in the following sections. The equations are linearized around the operating point and the state space model of the system is derived later.

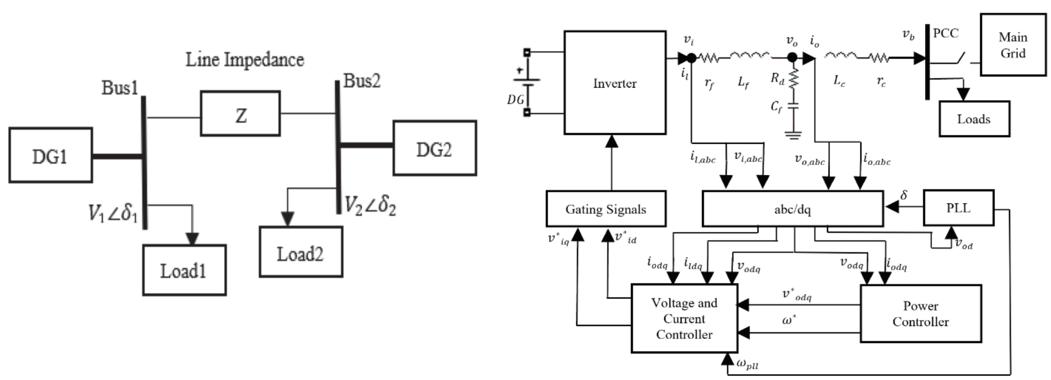

(**a**) (**b**)

Figure 1. (**a**) Microgrid Under Test; (**b**) DG System Block Diagram

2.1. Droop Control with Secondary Control Loop

In this work, the power controller is a droop control with a secondary control loop. A low pass filter is used to remove the higher harmonics of the instantaneous powers $\tilde{P}$ and $\tilde{Q}$. These instantaneous powers are calculated using inverter's output voltages and currents ($v_{od}, i_{id}, v_{oq}, i_{iq}$) as expressed in (1) and (2).

$$P = \frac{\omega_c}{s+\omega_c}\tilde{P} \Rightarrow \dot{P} = -P\omega_c + \underbrace{\left(v_{od}i_{id} + v_{oq}i_{iq}\right)}_{\tilde{P}}\omega_c \quad (1)$$

$$Q = \frac{\omega_c}{s+\omega_c}\tilde{Q} \Rightarrow \dot{Q} = -Q\omega_c + \underbrace{\left(v_{oq}i_{id} + v_{od}i_{iq}\right)}_{\tilde{Q}}\omega_c \quad (2)$$

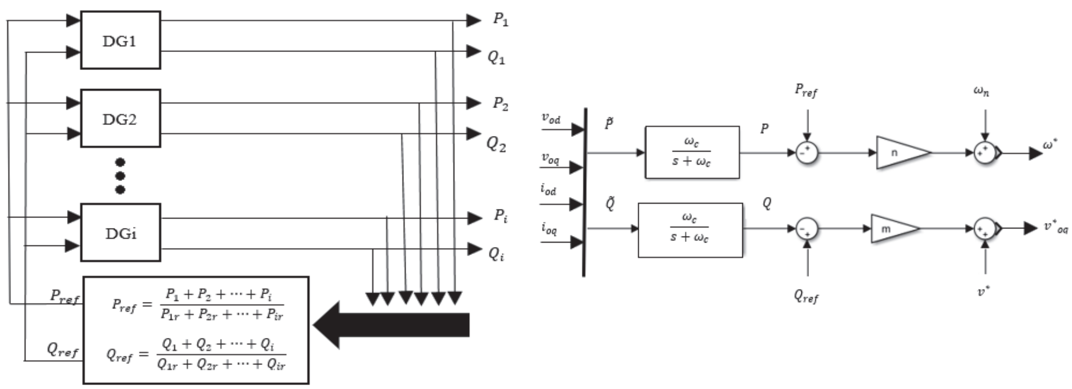

(**a**) (**b**)

Figure 2. (**a**) Secondary Control Loop [5]; (**b**) Power Controller with Droop Control

Figure 2(a) shows the secondary control loop design of the power controller used in the suggested MG [5]. The secondary control loop collects the power outputs P and Q of each inverter and then calculates the reference active/reactive powers according to the inverter's power ratings. In this work, the power ratings of the inverters are assumed to be equal ($P_{1r} = P_{2r}$) and the studied MG is considered as a low voltage MG. In the low voltage MGs, the output reactance is lower than the output resistance of the inverter. Therefore, a P-f/Q-V droop can be well-implemented, which is commonly used for low voltage MGs. The block diagram of the droop controller is presented in Figure 2(b) and the corresponding equations are shown in (3)-(4) for each of the DGs: (i = 1, 2)

$$\omega^*{}_i = \omega_n - n(P_{ref} - P_i) \tag{3}$$

$$v^*{}_{oqi} = v^* - m(Q_{ref} - Q_i) \tag{4}$$

2.2. *Phase Locked Loop (PLL)*

PLL is used to model the effects of load changes on the system's frequency. Figure 3(a) shows the PLL used for the small signal analysis of the DG system. This PLL is modeled in the dq-axis reference frame [7]. The input of the model is the d-axis voltage of the capacitor, C_f. The PLL tracks phase angle using a PI controller. The input of the PLL is the d-axis of the measured output voltage, and it is set to zero ($v_{od} = 0$). Also, the voltage of the load is considered to be in q-axis (v_{oq}). Following are the equations related to the design of the corresponding PLL:

$$\frac{dv_{odf}}{dt} = \omega_{cpll} v_{od} - \omega_{cpll} v_{odf} \tag{5}$$

$$\frac{d\phi_{pll}}{dt} = -v_{odf} \tag{6}$$

$$\frac{d\delta}{dt} = \omega_{pll} \tag{7}$$

$$\omega_{pll} = 120\pi - k_{p_{pll}} v_{odf} + k_{i_{pll}} \phi_{pll} \tag{8}$$

2.3. IMC-Based Voltage and Current Controller

Figure 3(b) shows the IMC-based voltage and current controller which uses PI, PD and PID controllers to control the output voltage and current of the filter along with the frequency of the system [3]. By using IMC, the system's output can be predicted through different control signals in the feed-forward loop. Another advantage of the IMC is that the set points can be changed using a feedback loop to balance out the different model mismatch and disturbances.

2.3.1. Voltage Controller

Mathematical modeling of the internal model-based voltage controller with filter dynamics is derived from [3]. The control parameters are described as below:

$$k_{pv} = \frac{C_f}{\lambda_v + R_d}, \qquad k_{dv} = \frac{T_c C_f}{\lambda_v + R_d}, \qquad k'_{pv} = \frac{\omega C_f T_c}{\lambda_v + R_d}, \qquad k'_{iv} = \frac{\omega C_f}{\lambda_v + R_d} \tag{9}$$

As shown in Figure 3(b), the reference frequency and the output voltage from the power controller are used as set-points for the voltage controller. The difference between droop frequency and the voltage from the load and their set-points are calculated and sent to the IMC voltage controller. ϕ_d and ϕ_q are the states of the IMC voltage controller. (10)-(13) show the equations related to the voltage controller.

$$\frac{d\phi_d}{dt} = \omega_{pll} - \omega^* \tag{10}$$

$$\frac{d\phi_q}{dt} = v^*{}_{oq} - v_{oq} \tag{11}$$

$$i^*{}_{lq} = \underbrace{\left(k_{p_v} + s k_{d_v}\right)}_{k_{pd_v}(s)} \left(v^*{}_{oq} - v_{oq}\right) + \underbrace{\left(k'{}_{p_v} + \frac{k'{}_{i_v}}{s}\right)}_{k'{}_{pi_v}(s)} \left(\omega_{pll} - \omega^*\right) \tag{12}$$

$$i^*{}_{ld} = \underbrace{\left(k_{p_v} + s k_{d_v}\right)}_{k_{pd_v}(s)} \left(\omega_{pll} - \omega^*\right) - \underbrace{\left(k'{}_{p_v} + \frac{k'{}_{i_v}}{s}\right)}_{k'{}_{pi_v}(s)} \left(v^*{}_{oq} - v_{oq}\right) \tag{13}$$

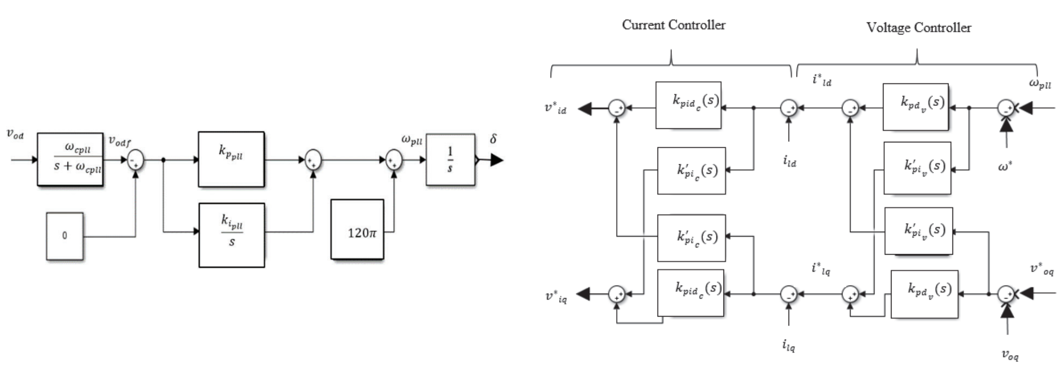

(**a**) (**b**)

Figure 3. (**a**) Phase Locked Loop Architecture; (**b**) IMC-Based Voltage and Current Controller

2.3.2. Current Controller

IMC current controller is designed and implemented using the same methods presented in [2-3]. As it is seen from Figure 3(b), the filtered currents (i_{ld}, i_{lq}) are compared with the voltage controller output (i^*_{ld}, i^*_{lq})) and then the error is sent to the current controller. The output of the integrator, γ_d and γ_q, are considered as the state variables. The corresponding differential equations and the control parameters of this controller are shown in (14)-(18).

$$k_{pc} = \frac{r_f T_{pwm} + L_f}{\lambda_c}, \qquad k_{ic} = \frac{r_f - T_{pwm} L_f \omega^2}{\lambda_c} \qquad k_{dc} = \frac{T_{pwm} L_f}{\lambda_c}, \qquad k'_{pc} = \frac{2\omega T_{pwm} L_f}{\lambda_c}$$
$$k'_{ic} = \frac{2(L_f + r_f T_{pwm})}{\lambda_c} \tag{14}$$

$$\frac{d\gamma_d}{dt} = {i^*}_{ld} - i_{ld} \tag{15}$$

$$\frac{d\gamma_q}{dt} = {i^*}_{lq} - i_{lq} \tag{16}$$

$${v^*}_{id} = \underbrace{\left(k_{p_c} + sk_{d_c} + \frac{k_{i_c}}{s}\right)}_{k_{pid_c}(s)}({i^*}_{ld} - i_{ld}) - \underbrace{({k'}_{p_c} + \frac{{k'}_{i_c}}{s})}_{{k'}_{pi_c}(s)}({i^*}_{lq} - i_{lq}) \tag{17}$$

$${v^*}_{iq} = \underbrace{\left(k_{p_c} + sk_{d_c} + \frac{k_{i_c}}{s}\right)}_{k_{pid_c}(s)}({i^*}_{lq} - i_{lq}) + \underbrace{({k'}_{p_c} + \frac{{k'}_{i_c}}{s})}_{{k'}_{pi_c}(s)}({i^*}_{ld} - i_{ld}) \tag{18}$$

2.4. LCL Filter

The LCL filter is shown in Figure 1(b). This filter is used to eliminate the higher harmonics. r_c and r_f are parasitic resistances of the inductor. The resistance of the capacitor is also incorporated in the resistor R_d. The method in [7] is used to design R_d. The filter equations are shown in (19)-(21):

$$\begin{cases} \dfrac{di_{ld}}{dt} = -\dfrac{r_f}{L_f} i_{ld} + \dfrac{1}{L_f} v_{id} - \dfrac{1}{L_f} v_{od} + \omega_{pll} i_{lq} \\ \dfrac{di_{lq}}{dt} = -\dfrac{r_f}{L_f} i_{lq} + \dfrac{1}{L_f} v_{iq} - \dfrac{1}{L_f} v_{od} - \omega_{pll} i_{ld} \end{cases} \tag{19}$$

$$\begin{cases} \dfrac{dv_{od}}{dt} = \dfrac{1}{C_f}(i_{ld} - i_{od}) + R_d\left(\dfrac{di_{ld}}{dt} - \dfrac{di_{od}}{dt}\right) + \omega_{pll} v_{oq} \\ \dfrac{dv_{oq}}{dt} = \dfrac{1}{C_f}(i_{lq} - i_{oq}) + R_d\left(\dfrac{di_{lq}}{dt} - \dfrac{di_{oq}}{dt}\right) - \omega_{pll} v_{od} \end{cases} \tag{20}$$

$$\begin{cases} \dfrac{di_{od}}{dt} = \dfrac{1}{L_f}(v_{od} - v_{bd} - i_{od} r_c) + \omega_{pll} i_{oq} \\ \dfrac{di_{oq}}{dt} = \dfrac{1}{L_f}(v_{oq} - v_{bq} - i_{oq} r_c) - \omega_{pll} i_{od} \end{cases} \tag{21}$$

2.5. Network and Load Model

As it is seen in Figure 1(a), Z represents the line impedance between the two microgrids. This impedance has a direct effect on the power sharing between the two inverters. The transmission line is mathematically modeled as below:

$$\begin{cases} \dfrac{di_{lineD1}}{dt} = \dfrac{1}{L_{line}}(v_{bD1} - v_{bD2} - i_{lineD1} R_{line}) + \omega i_{lineQ1} \\ \dfrac{di_{lineQ1}}{dt} = \dfrac{1}{L_{line}}(v_{bQ1} - v_{bQ2} - i_{lineQ1} R_{line}) - \omega i_{lineD1} \end{cases} \tag{22}$$

A static load including a combination of resistors and inductors is connected to each bus of the system. They are modeled using the following equations. For i = 1, 2 we have:

$$\begin{cases} \dfrac{di_{loadDi}}{dt} = \dfrac{1}{L_{loadi}}(v_{bDi} - i_{loadDi}R_{loadi}) + \omega_{pll}i_{loadQi} \\ \dfrac{di_{loadQi}}{dt} = \dfrac{1}{L_{loadi}}(v_{bQi} - i_{loadQi}R_{loadi}) - \omega_{pll}i_{loadDi} \end{cases} \tag{23}$$

Because the system frequency is constant, $\boldsymbol{\omega_{pll}}$ appears in the network and load equations. In the equations, the variables which have DQ as the subscript, are in the global reference frame. The first MG is considered as the reference frame for the whole study. The new phase angles for the DGs considering the reference frame, are presented in (24).

$$\begin{cases} \dot{\delta}_1 = \omega_{pll,1} - \omega_{pll,1} = 0 \\ \dot{\delta}_2 = \omega_{pll,2} - \omega_{pll,1} \end{cases} \tag{24}$$

3. Microgrid Model

The steady state operating point of the system is found by linearizing the nonlinear equations using *linear analysis tool* in MATLAB SIMULINK. The DG system model is then linearized around the operating point and the state space representation is obtained as (25).

$$\dot{\tilde{x}} = A\tilde{x} + B\tilde{u} \tag{25}$$

In this equation, u represents the input and consists of the following:

$$u = [v_{bD1} \;\; v_{bQ1} \;\; v_{bD2} \;\; v_{bQ2}]^T \tag{26}$$

In this microgrid every DG has 15 states. The load model has 4 states, and the network model has 2 states. Hence, the state space representation has 36 states in total. Matrix x in (27) represents the state variables.

$$x = [x_{inveter1} \;\; x_{inveter2} \;\; x_{line} \;\; x_{load}]^T \tag{27}$$

The bus voltages should also be considered in the system matrix (A) to accurately predict the load changes. In this respect, a large virtual resistor (R_N) is considered to have minimum effects on the dynamics of the system. By introducing R_N, the input matrix u is determined in terms of the states using (28).

$$\begin{cases} v_{bD1} = R_N(i_{oD1} - i_{loadD1} - i_{lineD12}) \\ v_{bQ1} = R_N(i_{oQ1} - i_{loadQ1} - i_{lineQ12}) \\ v_{bD2} = R_N(i_{oD2} - i_{loadD2} + i_{lineD12)} \\ v_{bQ2} = R_N(i_{oQ2} - i_{loadD2} + i_{lineD12}) \end{cases} \tag{28}$$

As previously discussed, MG1 is assumed as the reference. It is important to transform all the variables from their local reference to a global reference frame, because all the mathematical models were derived in each of the component's local frame. This transformation is carried out using (29).

$$\begin{cases} \begin{bmatrix} F_D \\ F_Q \end{bmatrix}_{Global} = \begin{bmatrix} \cos\delta & -\sin\delta \\ \sin\delta & \cos\delta \end{bmatrix} \begin{bmatrix} F_d \\ F_q \end{bmatrix}_{Local} \\ \begin{bmatrix} F_d \\ F_q \end{bmatrix}_{Local} = \begin{bmatrix} \cos\delta & \sin\delta \\ -\sin\delta & \cos\delta \end{bmatrix} \begin{bmatrix} F_D \\ F_Q \end{bmatrix}_{Global} \end{cases} \tag{29}$$

δ represents the phase angle between the global and the local reference frame. This equation is also linearized and incorporated to the system matrix.

4. Control Parameter Optimization

The eigenvalues of matrix A in the state space representation shown in (27), are the system's poles. By tuning the control parameters of the system, the critical control parameters are found. As it is shown in Figure 4(1)., the eigenvalue spectrum of matrix A can be divided into three frequency regions: high, medium, and low frequency. It is known that the control parameters related to the power controller are in the low frequency region. These parameters are also generally known as dominant mode. It is also demonstrated that the critical parameters concerning the IMC based voltage and current controllers are in the medium and high frequency regions.

The values of λ_v and λ_c are estimated and then tuned ($\lambda_v = 10^{-4}$ $\lambda_c = 10^{-5}$). In Table 1, the control parameters, and parameters of the microgrid are shown. In Figure 4(b) the eigenvalue analysis is presented by changing the "m" parameter of the droop controller. By repeating the same analysis for other control parameters, the domain of the critical parameters are obtained as follows: $n_p \in [10^{-5}, 10^{-3}]; m_q \in [10^{-5}, 10^{-2}]; K_e \in [1, 120]; k'_{pv} \in [6.72e-3, 0.25];$ $k'_{iv} \in [1, 105]; k_{pv} \in [0.01, 12]; k_{pc} \in [1,272]$. These domains will help to improve computational efficiency during the optimization process. It is noteworthy to mention that the other parameters do not have significant effects on the power sharing, stability, and resiliency of the system.

Table 1. Microgrid Parameters

Parameters	Value	Parameters	Value	Parameters	Value
k_{p_v}	0.34	ω_{cpll}	9420	R_{load1}	22.96 Ω
k_{d_v}	2.14e-4	L_f	1.35 mH	R_{load2}	25.0 Ω
k_{p_c}	23149	r_f	0.15 Ω	R_{line}	0.23 Ω
k_{i_c}	14334.47	C_f	1500 μF	L_{load1}	2.52 mH
k_{d_c}	0.008	L_c	0.35 mH	L_{load2}	5.37 mH
k'_{p_v}	1.51	r_c	0.03 Ω	L_{line}	0.32 mH
k'_{i_v}	31.72	$k_{i_{pll}}$	0.25	ω_c	37.68
k'_{p_c}	4.239	R_d	0.14	m	2.9e-4
k'_{i_c}	271.5	f_{sw}	10 kHz	n	3.1e-3
v^*	380	$k_{p_{pll}}$	8		

In this paper, Grey Wolf Optimizer [10] is used to optimize the parameters of the controllers. . This algorithm is inspired by the hierarchy and hunting methods of the grey wolves. The advantages of this method over other heuristic methods are that it is flexible and easy to implement, and it is applicable to different problems without any significant changes. Also, this method has a better exploration ability in comparison with other methods, especially in the power electronics applications.

Power sharing is an important aspect of the operation of the parallel inverters. Therefore, the objective is considered as a deviation from a reference reactive power (Q_{ref}). For the optimization, the objective presented in (32) is considered with the constraints shown in (33). A population size of 15 and an iteration number of 50 are assumed for the optimization. Figure 5 presents the objective function convergence with respect to the iterations.

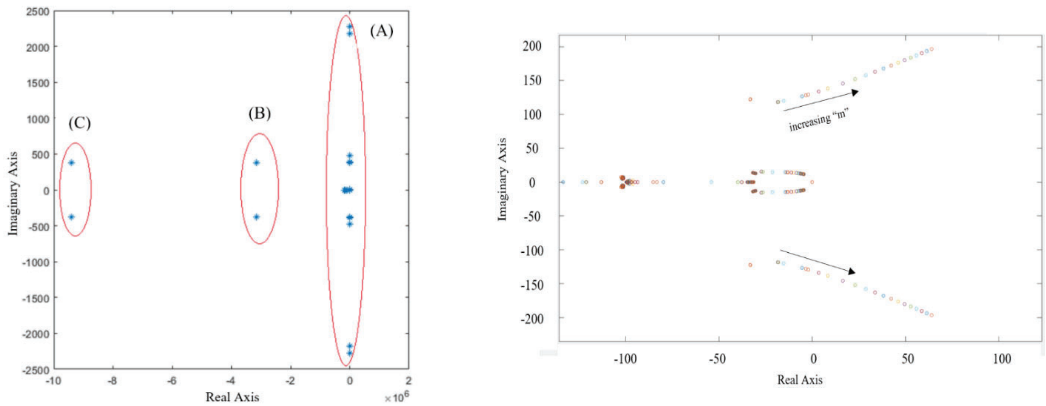

(**a**) (**b**)

Figure 4. (**a**) Eigenvalue Representation of the DG System; (**b**) Trace of system eigenvalues by increasing "m" from 10^{-6} to 10^{-2}

The derived optimal values for the critical parameters $n_p, m_q, K_e, k'_{pv}, k'_{iv}, k_{pv}, k_{pc}$ are: 0.008, 9.018e-05, 120, 0.133, 1.320, 20.240 and 283.6611, respectively. The derived optimal values for the critical parameters $n_p, m_q, K_e, k'_{pv}, k'_{iv}, k_{pv}, k_{pc}$ are: 0.008, 9.018e-05, 120, 0.133, 1.320, 20.240 and 283.6611, respectively.

$$\min F = \left(Q_m - Q_{ref}\right)^2 \tag{30}$$

$$\begin{gathered}
n_p^{min} \le n_p \le n_p^{max} \\
m_q^{min} \le m_q \le m_q^{max} \\
k_e^{min} \le k_e \le k_e^{max} \\
k'^{min}_{pv} \le k'_{pv} \le k'^{max}_{pv} \\
k'^{min}_{iv} \le k'_{iv} \le k'^{max}_{iv} \\
k_{pv}^{min} \le k_{pv} \le k_{pv}^{max} \\
k_{pc}^{min} \le k_{pc} \le k_{pc}^{max}
\end{gathered} \tag{31}$$

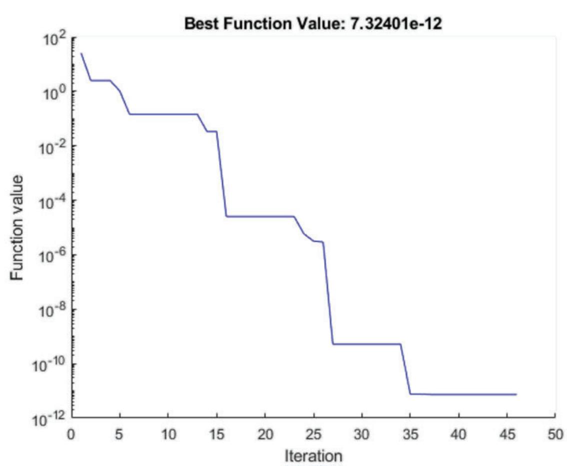

Figure 5. Optimization Convergence Plot

5. Simulation Results

An active load of 5kW is added to DG1 between 1s and 1.5s and another active load of 10kw is connected to DG2 between 1.5s and 2s.

Figure 6 shows the active and reactive power sharing between the two DGs using the proposed critical parameters in time-domain simulation. Equal power sharing between the DGs exists in steady-state condition. It is shown that from 1 to1.5 seconds, DG1 is sharing more power due to the increase of load 1. Similarly, DG2 is sharing more power from 1.5 to 2 seconds when load 2 is increased. The stability of the frequency and the q-axis voltage of the DGs are also presented in Figures 6(a) and 6 (b), respectively. It is shown that both voltage and frequency are regulated within the acceptable range. Figure 6 also shows that the stability of voltage and frequency is maintained by fast restoration, thus proving the improvement of the resiliency of the system.

In order to evaluate the performance of the proposed critical parameters of the system, two disturbances (a small and a large one) are applied. The results using the obtained critical parameters are shown in Table 2. The DGs' stability and resiliency performance are reported as rising time (t_r), overshoot (M_p) and settling time (t_s). For comparison, the same analysis is executed for the control parameters derived from the conventional methods and the results are presented in Table 3. For instance, the overshoot (M_p) for both DGs in case of small disturbance in Table 2 are much less than the overshoot of the DGs with small disturbance in Table 3. We can see the same improvement for the t_r and t_s indices in Table 2 in comparison with Table 3. Hence, the effectiveness of the proposed parameters identification method is verified.

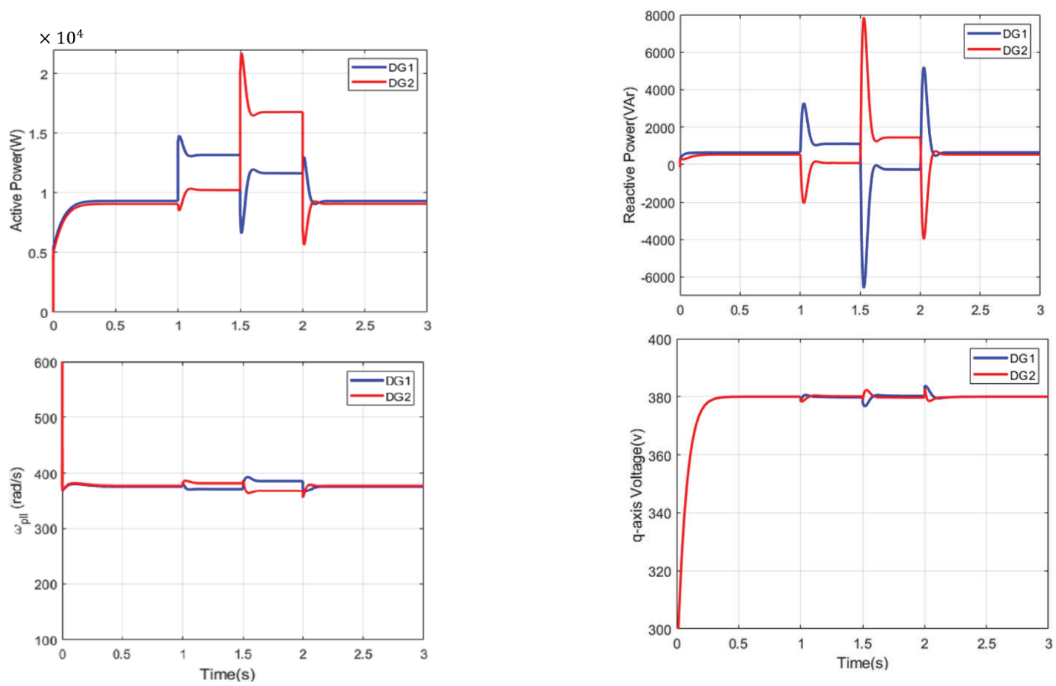

(**a**) (**b**)

Figure 6. (**a**) Active Power Sharing and Frequency Characteristics of the Two DGs; (**b**) Reactive Power Sharing and q-axis Voltage of the Two DGs

Table 2. Performance Evaluation of the Proposed Critical Parameters

Parameters	Small Disturbance 1-1.5s		Large Disturbance 1.5-2s	
	DG1	DG2	DG1	DG2
$t_r(s)$	0.0947 s	0.0942 s	0.011 s	0.013 s
$M_p(\%)$	0.98 %	0.23 %	2.47 %	1.7 %
$t_s(s)$	0.074 s	0.078 s	0.11 s	0.085 s

Table 3. Performance Evaluation of the Conventional Controllers

Parameters	Small Disturbance 1-1.5s		Large Disturbance 1.5-2s	
	DG1	DG2	DG1	DG2
$t_r(s)$	0.129 s	0.142 s	0.62 s	0.34 s
$M_p(\%)$	5.87 %	8.68 %	3.69 %	6.12 %
$t_s(s)$	0.69 s	0.63 s	0.141 s	0.158 s

Especially less settling time (t_s) in the critical parameters case shows fast restoration after applying the disturbances, and less overshoot (M_p) leads to less chance of damaging the equipment in the DG system while restoration. Consequently, the results show the improvement of the resiliency as well.

6. Conclusions and Future Work

In this work, the stability, resiliency and power sharing characteristics of IDGs comprising of a droop control with a secondary control loop and an IMC-based voltage and current controller is studied. Accurate mathematical modeling and equations of each of the mentioned components along with PLL, and the network and load models are discussed. The equations are then modeled using MATLAB, SIMULINK, after which an operating point is derived, and the equations are linearized around that operating point using the *Linear Analysis Tool*. The state space equations of the system are presented and the eigenvalue and sensitivity analysis of the IDG are presented using the system matrix (A). The critical parameters are identified, and stability domains of these parameters are presented. Moreover, a GWO algorithm is proposed to find the optimal control parameters and to improve the stability, resiliency, and power sharing in the system. Various load disturbances are applied in different time steps to show the effectiveness of the proposed GWO algorithm in the time domain simulations. Finally, different stability indices are calculated to verify the stability and resiliency of the DG system. The results show an improved performance in comparison to the DG system with conventional droop controller.

In our future work, the performance of the proposed IDG system will be compared with other control schemes. Also, different optimization techniques will be investigated.

Author Contributions: Conceptualization, Maryam Bahramipanah, Zagros Shahooei and Mohammad Alali; methodology, Mohammad Alali; software, Mohammad Alali; validation, Mohammad Alali, Zagros Shahooei and Maryam Bahramipanah; formal analysis, Mohammad Alali; investigation, Mohammad Alali; resources, Mohammad Alali; data curation, Mohammad Alali; writing—original draft preparation, Mohammad Alali; writing—review and editing, Maryam Bahramipanah and Zagros Shahooe; visualization, Mohammad Alali; supervision, Maryam Bahramipanah and

Zagros Shahooe; project administration, Maryam Bahramipanah; All authors have read and agreed to the published version of the manuscript

Data Availability Statement: The data that support the findings of this study are available from the corresponding author upon 357 reasonable request.

Conflicts of Interest: The authors declare no conflict of interest.

References

1. I. T. Force *et al.*, "Trends in Microgrid Control," vol. 5, no. 4, pp. 1905–1919, 2014.
2. R. Majumder, "Some Aspects of Stability in Microgrids," vol. 28, no. 3, pp. 3243–3252, 2013.
3. Q. C. Zhong and Y. Zeng, "Universal Droop Control of Inverters with Different Types of Output Impedance," IEEE Access, vol. 4, pp. 702–712, 2016.
4. N. Pogaku, S. Member, M. Prodanovic, T. C. Green, and S. Member, "Modeling, Analysis and Testing of Autonomous Operation of an Inverter-Based Microgrid," vol. 22, no. 2, pp. 613–625, 2007.
5. I. Chung et al., "Control Methods of Inverter-Interfaced Distributed Generators in a Microgrid System," vol. 46, no. 3, pp. 1078–1088, 2010.
6. M. A. Hassan and M. A. Abido, "Optimal Design of Microgrids in Autonomous and Grid-Connected Modes Using Particle Swarm Optimization," vol. 26, no. 3, pp. 755–769, 2011.
7. K. Yu, Q. Ai, S. Wang, J. Ni, and T. Lv, "Analysis and Optimization of Droop Controller for Microgrid System Based on Small-Signal Dynamic Model," vol. 7, no. 2, pp. 695–705, 2016.
8. J. Hu, J. Zhu, D. G. Dorrell, and J. M. Guerrero, "Virtual flux droop method - A new control strategy of inverters in microgrids," IEEE Trans. Power Electron., vol. 29, no. 9, pp. 4704–4711, 2014.
9. D. K. Dheer, N. Soni, and S. Doolla, "Sustainable Energy, Grids and Networks Improvement of small signal stability margin and transient response in inverter-dominated microgrids," Sustain Energy, Grids Networks, vol. 5, pp. 135–147, 2016.
10. D. K. Dheer, O. V. Kulkarni, S. Doolla, and A. K. Rathore, "Effect of Reconfiguration and Meshed Networks on the Small Signal Stability Margin of Droop-Based Islanded Microgrids," IEEE Trans. Ind. Appl., vol. 54, no. 3, pp. 2821–2833, 2018.
11. I. Chung et al., "Control Methods of Inverter-Interfaced Distributed Generators in a Microgrid System," vol. 46, no. 3, pp. 1078–1088, 2010.
12. K. Yu, Q. Ai, S. Wang, J. Ni, and T. Lv, "Analysis and Optimization of Droop Controller for Microgrid System Based on Small-Signal Dynamic Model," vol. 7, no. 2, pp. 695–705, 2016.
13. D. K. Dheer, N. Soni, and S. Doolla, "Sustainable Energy, Grids and Networks Improvement of small signal stability margin and transient response in inverter-dominated microgrids," Sustain. Energy, Grids Networks, vol. 5, pp. 135–147, 2016.
14. D. K. Dheer, S. Doolla, S. Bandyopadhyay, and J. M. Guerrero, "Electrical Power and Energy Systems Effect of placement of droop based generators in distribution network on small signal stability margin and network loss," Int. J. Electr. Power Energy Syst., vol. 88, pp. 108–118, 2017.
15. A. Elrayyah, F. Cingoz, Y. Sozer, and S. Member, "Construction of Nonlinear Droop Relations to Optimize Islanded Microgrid Operation," vol. 51, no. 4, pp. 3404–3413, 2015.
16. I. A. C. Microgrids et al., "Containment and Consensus-Based Distributed Coordination Control to Achieve Bounded Voltage and Precise Reactive Power Sharing in," vol. 53, no. 6, pp. 5187–5199, 2017.
17. N. Bottrell, S. Member, M. Prodanovic, T. C. Green, and S. Member, "Dynamic Stability of a Microgrid With an Active Load," vol. 28, no. 11, pp. 5107–5119, 2013.
18. X. Tang, W. Deng, and Z. Qi, "Investigation of the Dynamic Stability of Microgrid," vol. 29, no. 2, pp. 698–706, 2014.
19. A. Kahrobaeian, S. Member, Y. A. I. Mohamed, and S. Member, "Analysis and Mitigation of Low-Frequency Instabilities in Autonomous Medium-Voltage Converter-Based Microgrids With Dynamic Loads," vol. 61, no. 4, pp. 1643–1658, 2014.
20. E. S. N. P. Raju and T. Jain, "Impact of load dynamics and load sharing among distributed generations on stability and dynamic performance of islanded AC microgrids," Electr. Power Syst. Res., vol. 157, pp. 200–210, 2018, doi: 10.1016/j.epsr.2017.12.022.
21. M. Yazdanian and A. Mehrizi-Sani, "Internal model-based current control of the RL filter-based voltage-sourced converter," IEEE Trans. Energy Convers., vol. 29, no. 4, pp. 873–881, 2014.
22. S. Leitner, M. Yazdanian, A. Mehrizi-Sani, and A. Muetze, "Small-Signal Stability Analysis of an Inverter-Based Microgrid with Internal Model-Based Controllers," IEEE Trans. Smart Grid, vol. 9, no. 5, pp. 5393–5402, 2018.
23. M. Rasheduzzaman, J. A. Mueller, and J. W. Kimball, "An accurate small-signal model of inverter-dominated islanded microgrids using (dq) reference frame," IEEE J. Emerg. Sel. Top. Power Electron., vol. 2, no. 4, pp. 1070–1080, 2014.
24. Q. Zhong and S. Member, "Robust Droop Controller for Accurate Proportional Load Sharing Among Inverters Operated in Parallel," vol. 60, no. 4, pp. 1281–1290, 2013.
25. N. K. Vemula, S. K. Parida, and S. Member, "Small Signal Stability Assessment of an Inverter-Based Microgrid With Universal Droop and Internal Model-Based Controllers."
26. L. Lei, M. A. Elgendy, N. Wade, and S. Ethni, "Power sharing between parallel inverters by using droop control with a secondary control loop," PEDG 2019 - 2019 IEEE 10th Int. Symp. Power Electron. Distrib. Gener. Syst., pp. 653–658, 2019.

27. V. Naresh Kumar and S. K. Parida, "Parameter Optimization of Universal Droop and Internal Model Controller for Multi Inverter-Fed DGs Based on Accurate Small-Signal Model," In IEEE Access, Vol. 7, Pp. 101928-101940, 2019.
28. H. M. Goodarzi and M. H. Kazemi, “An Optimal Autonomous Microgrid Cluster Based on Distributed Generation Droop Parameter Optimization And Renewable Energy Sources Using an Improved Grey Wolf Optimizer,” Eng. Optim., Vol. 0, No. 0, Pp. 1–21, 2017.
29. J. Pombo and M. Calado, “Proportional Resonant Current Control and Output-Filter Design Optimization for Grid-Tied Inverters Using Grey Wolf Optimizer,” 2020.
30. A. Djerioui, A. Houari, M. Machmoum, M. Ghanes, T. Mesbahi And M. F. Benkhoris, "Grey Wolf Optimizer Based Predictive Torque Control for Electric Vehicle Applications," 2020 22nd European Conference on Power Electronics and Applications (Epe'20 Ecce Europe), 2020, Pp. P.1-P.5
31. R. Sanjay, T. Jayabarathi, T. Raghunathan, V. Ramesh And N. Mithulananthan, "Optimal Allocation of Distributed Generation Using Hybrid Grey Wolf Optimizer," In IEEE Access, Vol. 5, Pp. 14807-14818, 2017.
32. H. A. Hassan And M. Zellagui, “Application of Grey Wolf Optimizer Algorithm for Optimal Power Flow of Two-Terminal HVDC Transmission System,” Pp. 701–712, 2017, Doi: 10.15598/Aeee.V15i5.2110.
33. V. Krishnamurthy and A. Kwasinski, "Effects of Power Electronics, Energy Storage, Power Distribution Architecture, and Lifeline Dependencies on Microgrid Resiliency During Extreme Events," in *IEEE Journal of Emerging and Selected Topics in Power Electronics*, vol. 4, no. 4, pp. 1310-1323, Dec. 2016, doi: 10.1109/JESTPE.2016.2598648.
34. A. M. Mahfuz-Ur-Rahman, M. Rabiul Islam, K. M. Muttaqi and D. Sutanto, "An Energy Management Strategy with Advanced Power Electronic Converter and Control to Achieve Energy Resiliency and Minimum Operating Cost," *2020 IEEE Industry Applications Society Annual Meeting*, 2020, pp. 1-8, doi: 10.1109/IAS44978.2020.9334709.
35. S. M. Ferdous, G. M. Shafiullah, F. Shahnia, R. M. Elavarasan and U. Subramaniam, "Dynamic Frequency and Overload Management in Autonomous Coupled Microgrids for Self-Healing and Resiliency Improvement," in *IEEE Access*, vol. 8, pp. 116796-116811, 2020, doi: 10.1109/ACCESS.2020.3004185.

CHAPTER FIVE

RESILIENCE-ORIENTED OPTIMAL SIZING AND SITING OF ENERGY STORAGE SYSTEMS IN MULTI-MICROGRID DISTRIBUTION SYSTEMS

Abstract

Using Energy Storage Systems (ESSs) has been shown to be one of the most effective ways to increase the reliability and resiliency as well as energy balance in active distribution networks. In this chapter, a novel resilience- oriented algorithm is proposed for optimal siting, and sizing of ESSs in multi-microgrid distribution networks. Within this context, this chapter proposes a multi-objective procedure to minimize network loss and the energy flow costs. The proposed procedure takes into account the sensitivity analysis to model the investment costs in order to improve the resiliency of the microgrids. The proposed optimization problem, which is non-convex, nonlinear and mixed-integer problem is solved using novel heuristic methods including a two-stage iterative process. The first stage consists of a genetic algorithm which gives a primary solution to the place and size of the ESSs. The second stage evaluates the solutions from the first part by solving an AC optimal power flow. A benchmark multi-microgrid distribution system is used as the case study to analyze the effectiveness of the proposed methodology using different investment costs. Finally, a fault scenario is examined to evaluate the resiliency of the system.

Introduction

To reduce the carbon emission and increase the energy sustainability, Distributed Generations (DGs) based on renewable energy resources are utilized in the distribution networks. For instance, in the past decades a lot of wind farms and solar PV panels were installed to increase the penetration of renewable energy into the electricity grid. Although renewable energies provide a cleaner energy and decrease greenhouse gasses emissions, they pose some new challenges. These challenges can span from some issues like stability and line congestion to power quality and reactive power requirement [1] [2]-[4]. Energy Storage System (ESS) integration is introduced as a promising solution to address the issues arisen from the intermittent nature of distributed renewable energy sources (DRES) in order to improve the system's stability, reliability, resiliency [5]-[8].

Moreover, in [9] the wind rooftops are introduced as a way to provide energy for the local demand. [9], [10] show that placing ESSs is the best solution or problems like storing the excess energy and reducing the power flow congestion.

In this respect, one of the main problems associated with the use of ESSs is to find their optimal place and size in order to increase the system resilience.

In [11] a new energy management technique including economic strategies for operation of system and sizing of battery storage is proposed. The objective of this energy management technique is to minimize the total operation cost of an on-grid microgrid. Further, [12] proposes an optimal sizing and allocation of a battery-PV-wind-diesel hybrid energy system to minimize the total cost and reduce total emission as well as to increase the life cycle of the battery. Optimal sizing of battery storage system is also investigated in [13] for minimizing the power losses in the electrical distribution networks.

This chapter proposes a novel two-stage iterative algorithm for optimal planning of ESSs in order to improve the network loss and minimize the energy flow cost. Also, an investment cost is introduced based on the sensitivity analysis. In the first stage of the proposed method, the optimal size and location of the ESS units are obtained using the Genetic Algorithm (GA). A fitness function is then calculated using the solutions and the investment cost of the ESSs. The fitness is then evaluated using an optimal AC Optimal Power Flow (AC-OPF). The AC-OPF considers a multi-objective function consisting of improving the system resiliency and minimizing the cost of the exchanged energy with the utility grid.

The remainder of this chapter is organized as follows. Section 2 provides a detailed description of the problem formulation. In section 3, the benchmark multi-microgrid active distribution system is introduced and the proposed ESS planning method is investigated on this system considering a constant investment cost. The obtained results from the proposed optimization method are then presented using different tables and figures. Further, an investment cost is introduced based on the sensitivity analysis of the MGs and the improvement of the system resilience is demonstrated. Also, a fault scenario is considered to show the effectiveness of the proposed optimal planning of the ESSs. Finally, main conclusions and discussions of the future work are presented in section 4.

Problem Description

In active distribution network the problem is arisen from the fact that there is no direct control over non-dispatchable DGs. Therefore, the objective is to install a few numbers of ESSs in order to overcome the unpredictable and intermittent power generation from DGs. This paper will address the optimal location and size of the pre-determined amount ESS units in a multi-microgrid distribution system. The objective function of the proposed planning problem is presented in (1).

$$Objective = -W_{Loss}\Gamma_{loss} + W_{EP}\left(\sum_{t} C_t^E \, E_t\right) \tag{1}$$

It is assumed that the multi-microgrid system is connected to an external grid, and the hourly exchanged energy cost (C_t^E) is provided. Also, like [12], it is supposed that all the ESSs have the same operating and installing cost. The first term in (1) is related to the network loss. The second term in (1) corresponds to the total exchanged energy cost with the external grid.

The weighting coefficients in the objective function (W_{Loss}, W_{EP}) are calculated using the Analytical Hierarchy Process (AHP) [14],[15]. Global constrains of the problem are as follows: i) Maximum number of ESSs installed in each MG ii) ESSs capacity and operating constraints (such as, ESS capability curves and energy reservoir bounds) iii) Constraints of the AC-OPF.

The proposed problem is a mixed-integer, nonconvex and nonlinear problem. A hybrid approach consisting of an AC-OPF and a Genetic Algorithm (GA) is proposed to deal with the complexity of this problem. The general scheme of the proposed approach is presented in Fig. 1. As presented in the figure, for the master problem, a GA algorithm is used to find a first solution to the siting and sizing of the ESSs. After which a sub-problem is defined that involves a fitness function consisting of the GA solution and the AC-OPF objectives. More details about the AC-OPF and the GA are presented in the following sections.

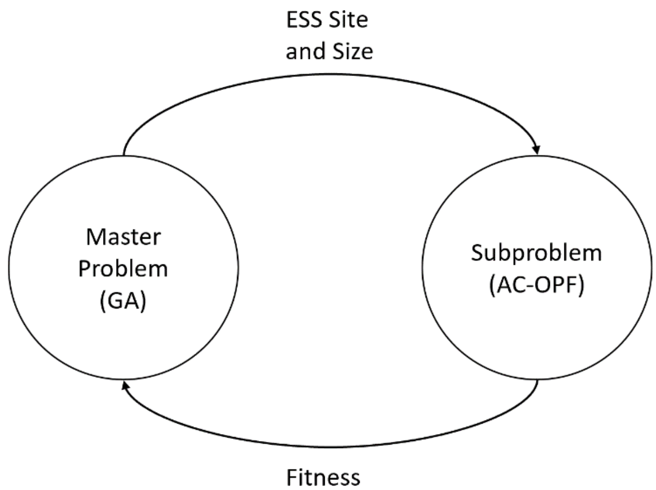

Fig. 1. The general Scheme of the suggested ESS Planning

Master Problem: Genetic Algorithm

The master problem finds the first optimal solution to the optimal siting and sizing of the ESS units. A GA approach is incorporated to find a solution to the optimization problem. The fitness value consists of the objective value of the subproblem (which is explained in the next subsection) and the investment cost of the ESS units. According to what was described previously, the GA fitness is presented in (2). In this equation, C_{inv} represents the investment cost and $Objective_{sub}$ is the objective for the subproblem. Three constraints are considered for the master problem: (i) the total capacity of ESSs which can be installed in each node (ii) the total ESSs capacity which is available (iii) maximum number of nodes that the ESSs can be installed.

$$F_{GA} = C_{Inv} + Objective_{sub} \tag{2}$$

The Objective Function

The objective function uses the solution from the master problem and performs a daily AC-OPF with the objectives introduced in (1) and then returns value to the master problem (Fig. 1).

As described, the objective is shown in (1). The constraints for the subproblem consist of: (i) the upper and lower voltage limits and the load balance equations known from the power flow (3)-(5) (ii) the ESS constraints (6)-(10).

$$V_{i,t} \sum_{j} (V_{j,t} \big(G_{i,j} \, sin\big(\delta_{i,t} - \delta_{j,t}\big)\big) - B_{i,j} \, cos\big(\delta_{i,t} - \delta_{j,t}\big)) = Q_{G_{i,t}} + Q_{ESS_{i,t}} - Q_{L_{i,t}} \tag{3}$$

$$V_{i,t} \sum_{j} (V_{j,t} \big(G_{i,j} \, cos\big(\delta_{i,t} - \delta_{j,t}\big)\big) + B_{i,j} \, sin\big(\delta_{i,t} - \delta_{j,t}\big)) = P_{G_{i,t}} + P_{ESS_{i,t}} - P_{L_{i,t}} \tag{4}$$

$$V_{min} \le V_{i,t} \le V_{max} \tag{5}$$

The maximum amount of energy that can be stored or taken from an ESS are demonstrated in equations (6) and (7). It is important to mention that in this work, it is assumed that the absorption and the generation of power do not change the energy reservoir level (this assumption is logical since most power converters have a high efficiency in the current AC grids).

$$\sum_{t'=0} P_{ESS_i}^{t'} \Delta t \, \eta_i \le E_{ESS_i}^{0} \quad \forall t, t = 1,2, \dots ,24 \tag{6}$$

$$\sum_{t'=0} -P_{ESS_i}^{t'} \Delta t \, \eta_i \leq E_{ESS_i}^{max} - E_{ESS_i}^{0} \; t = 1,2, \dots ,24 \tag{7}$$

$$E_{ESS_i}^{min} \leq E_{ESS_i}^{t} \leq E_{ESS_i}^{max} \tag{8}$$

$$P_{ESS_i}^{min} \leq P_{ESS_i}^{t} \leq P_{ESS_i}^{max} \tag{9}$$

$$(P_{ESS_i}^{t})^2 + (Q_{ESS_i}^{t})^2 \leq (C_{ESS_i}^{max})^2 \tag{10}$$

Equations (8) and (9) are related to the maximum and minimum energy and real power rating of the ESS units. Finally, equation (10) defines the limit for the maximum capability curve of the ESSs. Since the it is assumed that power converters are used in the grid, the capability curve will be limited by the ampacity of the of the power converter. In this work, the AC grid voltage is considered to be constant; so, the ampacity could be translated to the apparent power of the ESS [15].

Simulation and Results

A benchmark multi-microgrid system is used to evaluate the proposed scheme (Fig. 2). Full details and specification of each MG is presented in [16].

In this work, it is assumed that the synchronous generators and the wind turbines are not functional. The loads are only supplied by the non-dispatchable distributed generations (DGs) using the PV panels. In case the PV generation is not enough, the loads will be supplied by the energy bought from the utility grid.

The loads in this study are voltage independent PQ absorbers. The total active and reactive load of each one of the MGs are presented in Fig. 3. The same load pattern is assumed for each MG; however, the amount has been scaled according to the size of the corresponding MG. Also, the total PV generation is presented in Fig. 4. The reactive power injective of the PVs are considered to be zero. loads and the PV generation are presented for a winter day and a base power of 500 kVA is considered for this study.

The PV blocks in Fig. 2 shows the buses with incorporated PV generation. It is assumed that in each MG maximum number of 3 ESSs can be installed. Also, the total ESS power is considered to be 600 kW with a relevant energy capacity of 3MWh. Moreover, an efficiency of 80% is considered for the charging/discharging modes.

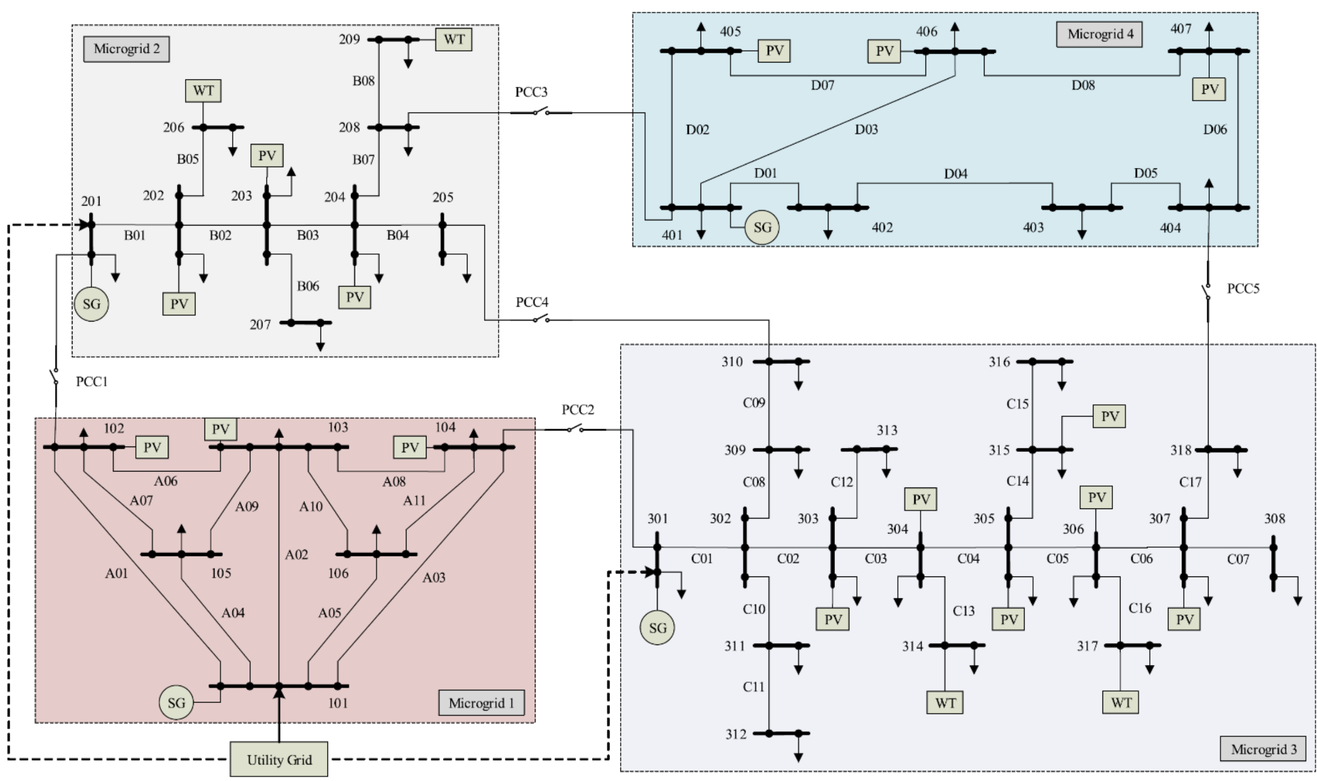

Fig. 2. The benchmark multi-microgrid system [16]

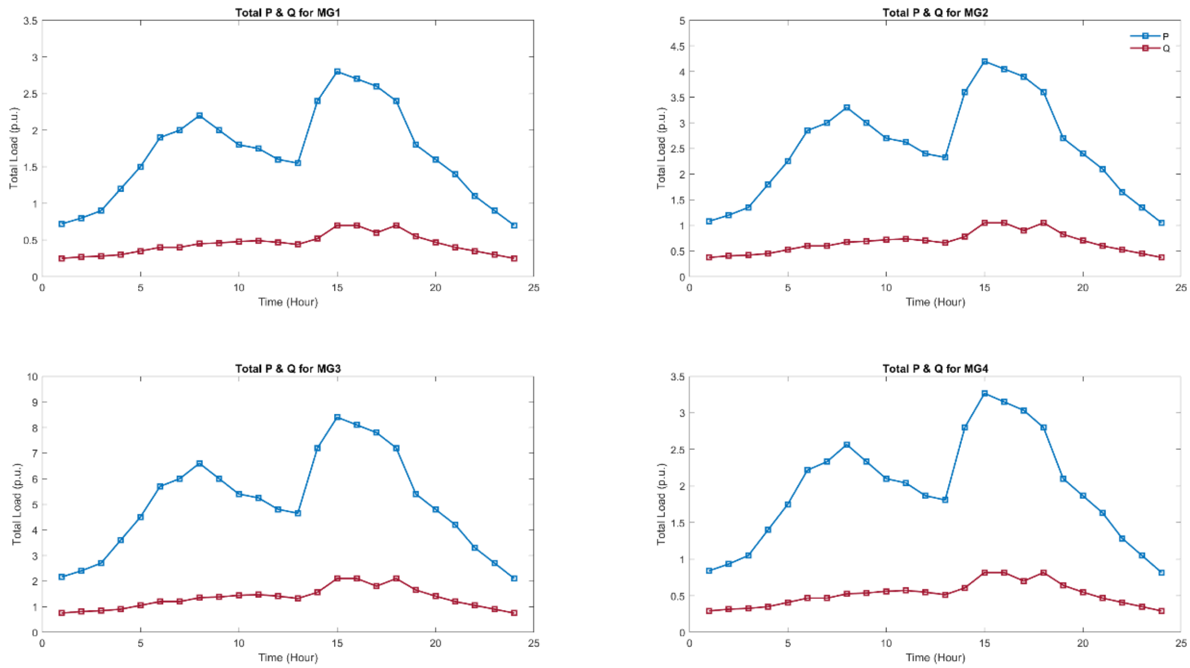

Fig. 3. Load profiles of each MG system

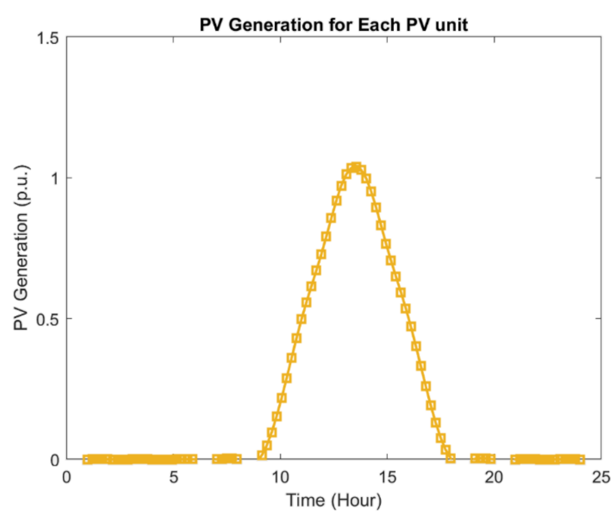

Fig. 4. PV generation for the PV used in the multi-MG system

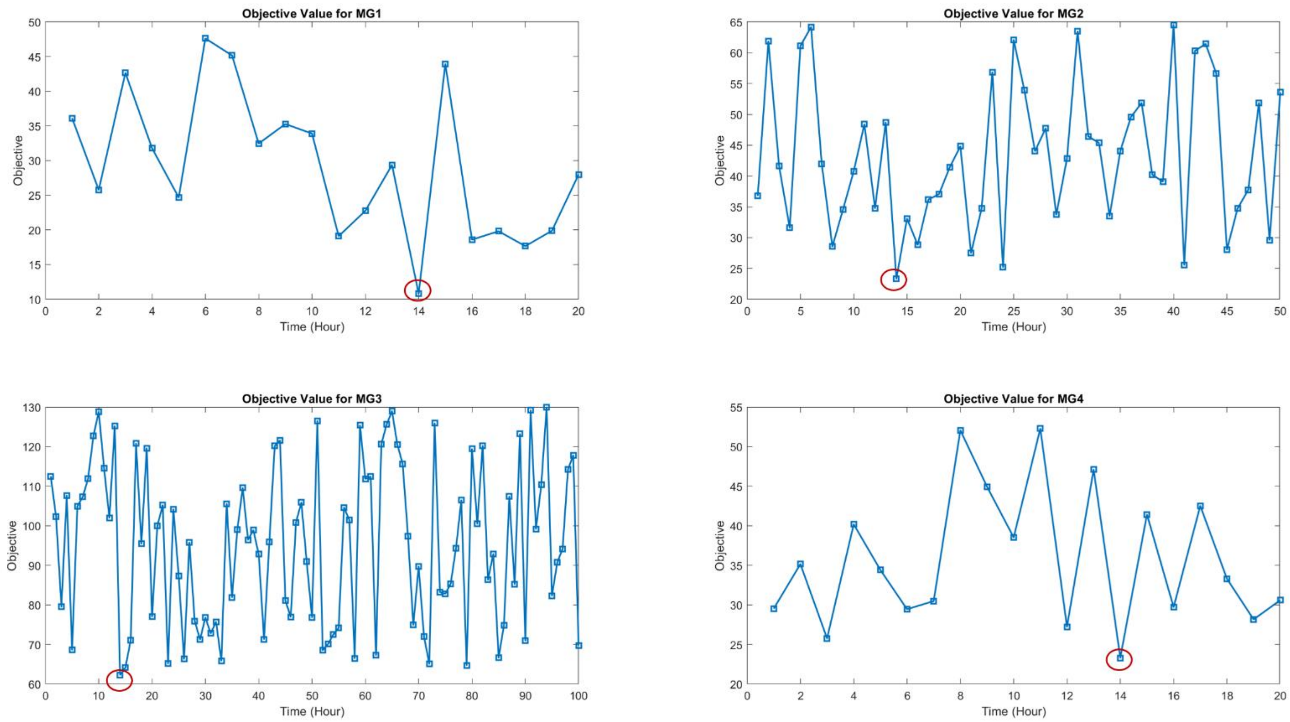

Fig. 5. Changes of the objective function due to keeping the sizing constant and randomly changing the siting

ESS Placement with Constant Investment Cost

The optimization problem is solved for each one of the MGs individually considering a constant investment cost of 5000 $/unit and the results for the optimal place and size of the ESSs are presented in Table 1. Moreover, in Table 2, for each MG, the objective values are shown for both with and without the optimal ESS allocation. As presented in the table, by using the optimal planning of the ESS, there will be major improvements in the values of loss and the cost of energy. To evaluate the effectiveness of the algorithm even further, the siting of the ESSs were randomly changed while keeping the sizing constant. The changes of the objective are brought in Fig. 5. The red circle in each plot represents the optimal siting that was derived using the proposed scheme.

As can be seen, the case represented by the red circle also has the minimum objective value, hence proving that it's the optimal case as suggested by the proposed method.

Table 1. Optimal Siting and Sizing of The ESS Units with Constant Investment Cost

MG1			
Bus number	101	105	106
Power Rating (kW)	234	266	100
Capacity (MWh)	1.1	1.3	0.6
MG2			
Bus number	209	205	206
Power Rating (kW)	180	220	200
Capacity (MWh)	0.7	1.2	1.1
MG3			
Bus number	310	318	316
Power Rating (kW)	230	160	210
Capacity (MWh)	1.15	0.8	1.05
MG4			
Bus number	403	404	402
Power Rating (kW)	240	270	90
Capacity (MWh)	1.1	1.3	0.6

ESS Placement with Investment Cost based on Sensitivity Analysis

In the last case, the investment cost was considered a constant value for every bus. To improve upon this and consider the voltage stability of the MGs, an investment cost based on the voltage sensitivity analysis is introduced below.

Voltage Sensitivity Coefficients ($VSCs$) are calculated for the sensitivity analysis of the grid. For a given operating state Φ, sensitivity matrix for active power ($[VSC^P]_{B\times N}$) is calculated whose

Table 2. Cost of Energy and Loss Before and After the ESS Planning with Constant Investment Cost

MG1		
Objective	**Loss (MWh/day)**	**Cost of Energy ($/day)**
Without ESS	2.6	64
With Optimal ESS Allocation	1.8	9
MG2		
Objective	**Loss (MWh/day)**	**Cost of Energy ($/day)**
Without ESS	3.4	92
With Optimal ESS Allocation	2.3	21
MG3		
Objective	**Loss (MWh/day)**	**Cost of Energy ($/day)**
Without ESS	8.2	167
With Optimal ESS Allocation	4.3	58
MG4		
Objective	**Loss (MWh/day)**	**Cost of Energy ($/day)**
Without ESS	17	72
With Optimal ESS Allocation	8.3	15

elements are defined in (11) where N is the set of all the network nodes and B is the set of all the PV nodes. VSC is defined as:

$$VSC_{i\rightarrow j}^{P} = \frac{\partial V_j}{\partial P_i}|_{\Phi} \; ; i \in B; j \in N \tag{11}$$

As an example, the calculated VSC^P for MG1 is shown below:

$$VSC^P = \begin{bmatrix} 0.02 & 0.32 & 0.024 & 0.16 & 0.1 & 0.08 \\ 0.07 & 0.19 & 0.29 & 0.033 & 0.11 & 0.04 \\ 0.1 & 0.2 & 0.23 & 0.3 & 0.03 & 0.12 \end{bmatrix}$$

As can be seen, in the first row, the fourth coefficient has the largest amount. This means that in MG1, the PV on bus 102 will mostly affect the voltage of bus 104. Therefore, less investment cost should be considered for this bus. So, by deriving VSC^P in each MG, the influence of each PV bus on the other buses can be interpreted.

Table 3. Optimal Siting and Sizing of The ESS Units with Investment Cost Based on Sensitivity Analysis

MG1			
Bus number	102	103	104
Power Rating (kW)	230	270	100
Capacity (MWh)	1	1.4	0.6
MG2			
Bus number	202	205	208
Power Rating (kW)	190	210	200
Capacity (MWh)	0.8	1.1	1.1
MG3			
Bus number	303	315	317
Power Rating (kW)	230	170	200
Capacity (MWh)	1.15	0.9	0.95
MG4			
Bus number	405	406	407
Power Rating (kW)	230	275	95
Capacity (MWh)	1.1	1.25	0.65

The bus with the most sensitivity should have the least investment cost to encourage the operators to install ESSs on the buses that need it most. Thus, the new investment cost is defined as a logarithmic function as shown in (12). The trend of the new investment cost is also demonstrated in Fig. 6. The optimal siting and sizing of the ESS units with the new investment cost is shown in Table 3. Moreover, the cost of energy and loss are also brought in Table 4.

$$New\ Investment\ Cost = -\log_2(VSC^P) \tag{12}$$

Table 4. Cost of Energy and Loss Before and After the ESS Planning with Investment Cost Based on Sensitivity Analysis

MG1		
Objective	**Loss (MWh/day)**	**Cost of Energy ($/day)**
Without ESS	2.6	64
With Optimal ESS Allocation	1.5	6
MG2		
Objective	**Loss (MWh/day)**	**Cost of Energy ($/day)**
Without ESS	3.4	92
With Optimal ESS Allocation	2.15	25
MG3		
Objective	**Loss (MWh/day)**	**Cost of Energy ($/day)**
Without ESS	8.2	167
With Optimal ESS Allocation	4.2	42
MG4		
Objective	**Loss (MWh/day)**	**Cost of Energy ($/day)**
Without ESS	17	72
With Optimal ESS Allocation	6.9	9

To verify the effectiveness of the new investment cost, the voltage profile of MG1 during normal operation is shown in three cases: **I)** Without the ESS units (Fig. 7 (a)) **II)** With ESS units and constant investment cost (Fig. 7 (b)) **III)** With ESS units and investment cost based on the voltage sensitivity analysis (Fig. 7 (c)). As demonstrated in the figures, Fig. 7 (c) (with the new investment cost) shows a more stable voltage on all the buses in comparison to the other two cases.

Fault Scenario

For further performance evaluation, a fault scenario is tested for MG1. The PVs on buses 102 and 103 are assumed to be out of work. The voltage profile of MG1 is again shown in three cases: **I)** Without the ESS units (Fig. 8 (a)) **II)** With ESS units and constant investment cost (Fig. 8 (b)) **III)** With ESS units and investment cost based on the voltage sensitivity analysis (Fig. 8 (c)). As can be seen in Fig. 8(c), the voltage profile in presence of the ESSs and the new investment cost is more stable than the other two cases and MG1's resiliency has been improved using the optimal siting and sizing of the ESSs.

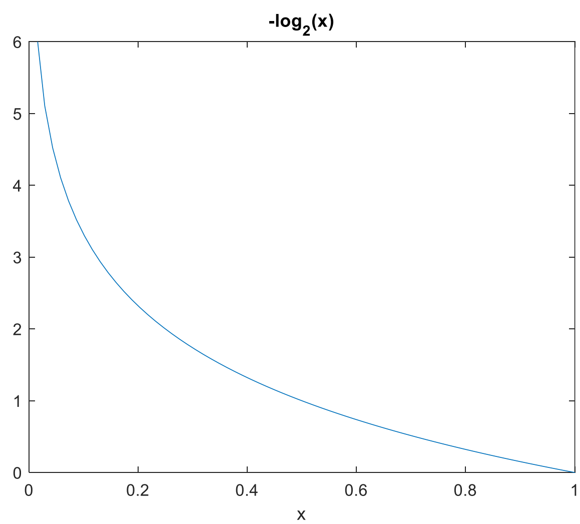

Fig. 6. The trend of the new investment cost

Conclusion and Future Work

This paper discusses a planning optimization problem relating to siting and sizing of the

ESSs with the goal of minimizing the network loss and energy cost from the grid in a multi-microgrid system.

The mentioned problem is a mixed-integer, nonlinear and non-convex problem. Due to the complexity of this problem, a two-stage process is introduced. The two stage iterative process consists of two parts: (i) the first part, a GA algorithm is used to find the site and size of the ESS units (ii) in the second stage, the fitness of the first part is evaluated using an AC-OPF.

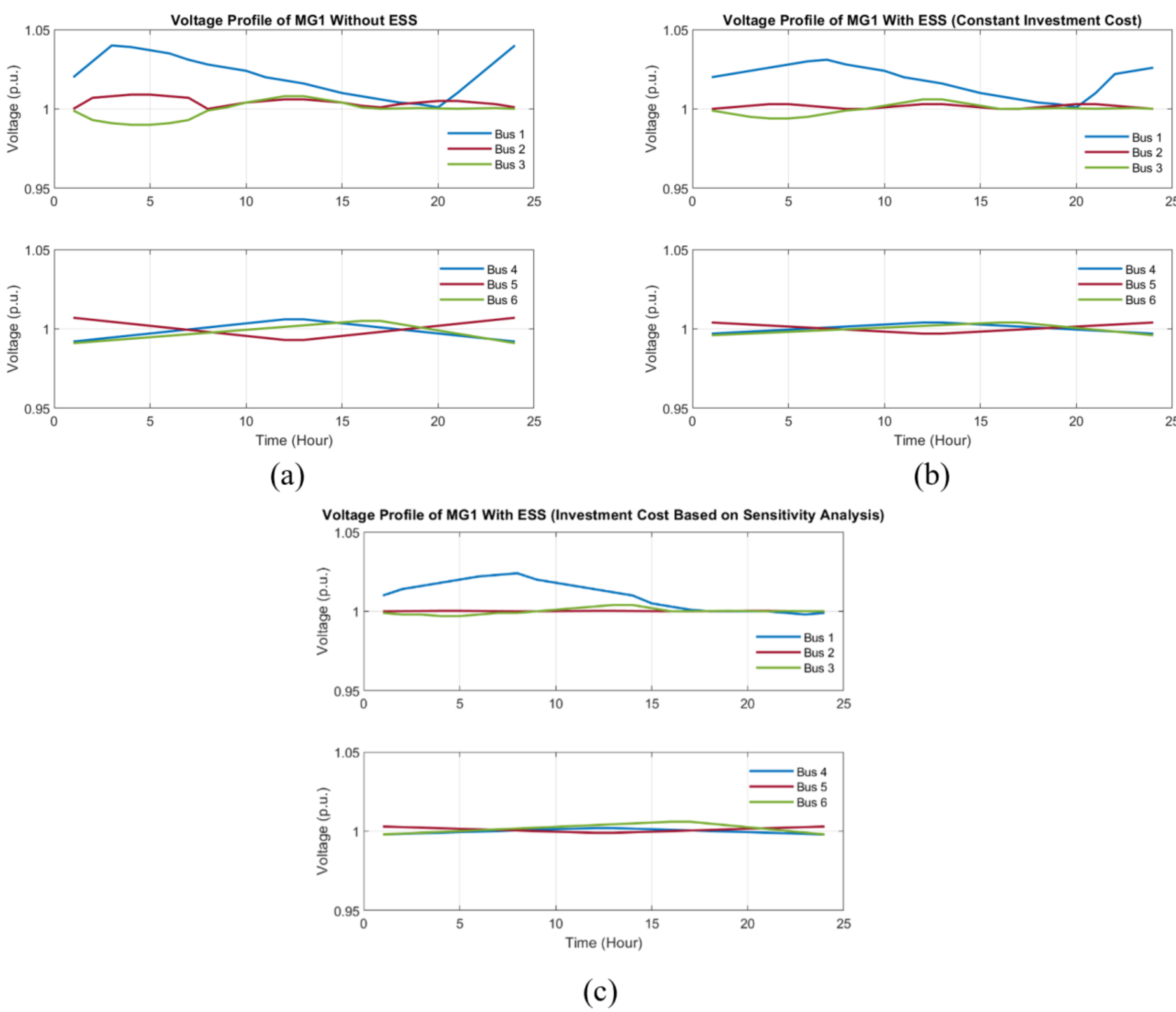

Fig. 7. Voltage profiles of MG1 in normal operation (a) without ESS (b) with ESS and constant investment cost (c) with ESS and investment cost based on sensitivity analysis

A benchmark multi-microgrid system is studied to show the effectiveness of the proposed method to find the optimal allocation of the ESSs. In this study, loads and PV absorption and generation has been considered for a winter day. Also, two investment costs are considered for the simulation: one constant and another one based on the voltage sensitivity analysis. The results from applying the proposed scheme has shown major improvements in the objectives which were considered, namely the network loss and the exchange energy cost with the utility grid. As a result, the proposed method has shown to be effective to increase the resiliency and improve the energy balance.

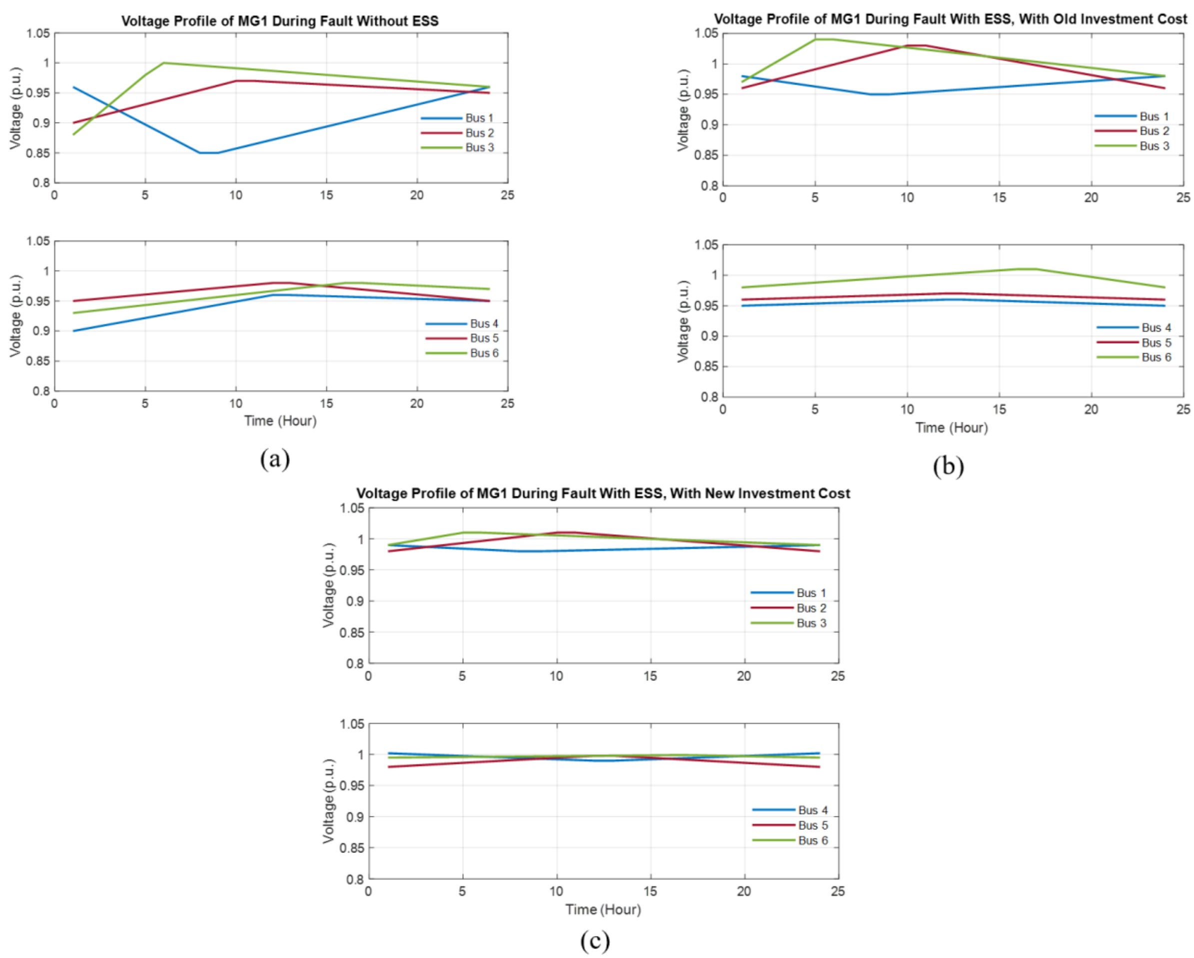

Fig. 8. Voltage profiles of MG1 during fault (a) without ESS (b) with ESS and constant investment cost (c) with ESS and investment cost based on sensitivity analysis

Overall, the investment cost based on the sensitivity analysis had a better performance in maintaining the voltage stability and improving the resiliency of the system. A fault scenario was also examined to verify the performance of the ESSs' siting and sizing.

In our future work, we will consider different resiliency indices along with different scenarios. Also, instead of considering a fixed number of ESSs for each MG, an optimization problem for the number of ESSs will be conducted in a form of multilevel optimization. Finally, a scheme will be investigated to implement the optimization problem for the whole multi-MG system rather that optimizing each MG individually.

References

[1] M. Farhoodnea, A. Mohamed, H. Shareef, and H. Zayandehroodi, "Power quality impacts of high-penetration electric vehicle stations and renewable energy-based generators on power distribution systems," *Meas. J. Int. Meas. Confed.*, vol. 46, no. 8, pp. 2423–2434, 2013.

[2] V. H. M. Quezada, J. R. Abbad, and T. G. San Román, "Assessment of energy distribution losses for increasing penetration of distributed generation," *IEEE Trans. Power Syst.*, vol. 21, no. 2, pp. 533–540, 2006

[3] N. Miller and Z. Ye, "Report on Distributed Generation Penetration Study," 2003.

[4] NREL, "DG Power Quality, Protection and Reliability Case Studies Report," 2003.

[5] G. Carpinelli, G. Celli, S. Mocci, F. Mottola, F. Pilo, and D. Proto, "Optimal Integration of Distributed Energy Storage Devices in Smart Grids," *IEEE Trans. Smart Grid*, vol. 4, no. 2, pp. 985–995, Jun. 2013.

[6] N. Jayasekara, P. Wolfs, and M. A. S. Masoum, “An optimal management strategy for distributed storages in distribution networks with high penetrations of PV,” *Electr. Power Syst. Res.*, vol. 116, pp. 147–157, Nov. 2014.

[7] H. Nazaripouya, Y. Wang, P. Chu, H. R. Pota, and R. Gadh, “Optimal sizing and placement of battery energy storage in distribution system based on solar size for voltage regulation,” in *2015 IEEE Power & Energy Society General Meeting*, 2015, pp. 1–5.

[8] E. Hooshmand and A. Rabiee, “Robust model for optimal allocation of renewable energy sources, energy storage systems and demand response in distribution systems via information gap decision theory,” *IET Gener. Transm. Distrib.*, vol. 13, no. 4, pp. 511–520, 2019.

[9] A. W. Bizuayehu, A. A. Sanchez de la Nieta, J. Contreras, and J. P. S. Catalao, “Impacts of Stochastic Wind Power and Storage Participation on Economic Dispatch in Distribution Systems,” *IEEE Trans. Sustain. Energy*, vol. 7, no. 3, pp. 1336–1345, Jul. 2016.

[10] A. Karimi, F. Aminifar, A. Fereidunian, and H. Lesani, “Energy storage allocation in wind integrated distribution networks: An MILP-Based approach,” *Renew. Energy*, vol. 134, pp. 1042–1055, Apr. 2019.

[11] S. Sukumar, H. Mokhlis, S. Mekhilef, K. Naidu, and M. Karimi, “Mix-mode energy management strategy and battery sizing for economic operation of grid-tied microgrid,” *Energy*, vol. 118, pp. 1322–1333, 2017

[12] A. S. O. Ogunjuyigbe, T. R. Ayodele, and O. A. Akinola, “Optimal allocation and sizing of PV/Wind/Split-diesel/Battery hybrid energy system for minimizing life cycle cost, carbon emission and dump energy of remote residential building,” *Appl. Energy*, vol. 171, pp. 153–171, 2016,

[13] R. V. A. Monteiro, G. C. Guimarães, F. A. M. Moura, M. R. M. C. Albertini, and F. B. Silva, “Long-term sizing of lead–acid batteries in order to reduce technical losses on distribution networks: A distributed generation approach,” *Electr. Power Syst. Res.*, vol. 144, pp. 163–174, 2017

[14] Z. Liu, F. Wen, G. Ledwich, "Optimal siting and sizing of distributed generators in distribution systems considering uncertainties," *IEEE Trans. Power Delivery*, vol. 26, pp. 2541-2551, Oct. 2011.

[15] Thomas L. Saaty ‘Decision making — the Analytic Hierarchy and Network Processes (AHP/ANP) ‘*Journal of Systems Science and Systems Engineering*, vol. 13, pp. 1-35, Mar. 2004,

[16] M. N. Alam, S. Chakrabarti, and X. Liang, “A Benchmark Test System for Networked Microgrids,” *IEEE Trans. Ind. Informatics*, vol. 16, no. 10, pp. 6217–6230, 2020

REFERENCES CITED

N. I. Yusoff, A. A. M. Zin, and A. B. Khairuddin, "Congestion management in power system: A review," in 2017 3rd International Conference on Power Generation Systems and Renewable Energy Technologies (PGSRET), April 2017, pp. 22–27.

"Dispatch of generation and demand side response in regional grids," 2015 IEEE 15th International Conference on Environment and Electrical Engineering, EEEIC 2015 - Conference Proceedings, pp. 482–486, 2015.

H. Emami and J. A. Sadri, "Congestion Management of Transmission Lines in the Market Environment," International Research Journal of Applied and Basic Sciences, vol. 3, pp. 2572–2580, 2012.

J. S. Rao and J. Amarnath, "Transmission Congestion Management Comparative Studies In Restructured Power System," International Journal of Scientific & Engineering Research, vol. 4, no. 8, pp. 177–182, 2013.

E. Dehnavi and H. Abdi, "Determining optimal buses for implementing demand response as an effective congestion management method," IEEE Transactions on Power Systems, vol. 32, no. 2, pp. 1537–1544, March 2017.

J. Wu, B. Zhang, and Y. Jiang, "Optimal day-ahead demand response contract for congestion management in the deregulated power market considering wind power," IET Generation, Transmission Distribution, vol. 12, no. 4, pp. 917–926, 2018.

V. K. Prajapati and V. Mahajan, "Reliability assessment and congestion management of power system with energy storage system and uncertain renewable resources," Energy, vol. 215, p. 119134, 2021.

M. A. Fotouhi Ghazvini, G. Lipari, M. Pau, F. Ponci, A. Monti, J. Soares, R. Castro, and Z. Vale, "Congestion management in active distribution networks through demand response implementation," Sustainable Energy, Grids and Networks, vol. 17, p. 100185, 2019.

A. Asrari, M. Ansari, and K. C. Bibek, "Real-time congestion prevention in modern distribution power systems via demand response of smart
homes," in 2019 North American Power Symposium (NAPS), 2019, pp. 1–6.

S. Y. Hadush and L. Meeus, "Dso-tso cooperation issues and solutions for distribution grid congestion management," Energy Policy, vol. 120, pp. 610 – 621, 2018.

S. Sharma and L. Srivastava, "Prediction of transmission line overloading using intelligent technique," Applied Soft Computing, vol. 8, no. 1, pp. 626 – 633, 2008.

A. M. Glazunova, "Forecasting power system state variables on the basis of dynamic state estimation and artificial neural networks," pp. 470–475, Jly 2010.

O. Ivanov, M. Gavrilas¸, and B. Neagu, "Intelligent monitoring and control in transmission and distribution networks," pp. 185–191, May 2014.

R. Fainti, M. Alamaniotis, and L. H. Tsoukalas, "Three-phase congestion prediction utilizing artificial neural networks," IISA 2016 - 7th International Conference on Information, Intelligence, Systems and Applications, pp. 1–5, 2016.

J. J. Mor´e, "The levenberg-marquardt algorithm: Implementation and theory," in Numerical Analysis, G. A. Watson, Ed. Berlin, Heidelberg: Springer Berlin Heidelberg, 1978, pp. 105–116.

J. Nocedal and S. J. Wright, Numerical Optimization, 2nd ed. New York, NY, USA: Springer, 2006.

F. Burden and D. Winkler, "Bayesian regularization of neural networks," Methods in molecular biology (Clifton, N.J.), vol. 458, pp. 23–42, 01 2009.

E. Sariev and G. Germano, "Bayesian regularized artificial neural networks for the estimation of the probability of default," Quantitative
Finance, pp. 1–18, 10 2019.

W. H. Kersting, "Radial distribution test feeders," IEEE Transactions on Power Systems, vol. 6, no. 3, pp. 975–985, 1991.

A. Chaouachi, R. Kamel, R. Andoulsi, and K. Nagasaka, "Multiobjective intelligent energy management for a microgrid," IEEE Trans. Indust. Elec., vol. 60, pp. 1688–1699, Apr. 2013.

R. Lasseter, "Microgrids," Proc. IEEE Power Eng. Society Trans. And Dist. Conf., vol. 1, pp. 305 – 308, Jan. 2002.

C. Schwaegerl, "Advanced architectures and control concepts for more microgrids," More Microgrids, Siemens AG, STREP, no. 1, pp. 1–145, 2009.

A. Kaur, J. Kaushal, and P. Basak, "A review on microgrid central controller," Renew. Sustain. Energy Rev., vol. 55, pp. 338–345, 2016.

W. Su, J. Wang, and J. Roh, "Stochastic energy scheduling in microgrids with intermittent renewable energy resources," IEEE Trans. Smart Grid, vol. 5, pp. 13–27, 2013.

T. Nguyen and M. Crow, “Stochastic optimization of renewable-based microgrid operation incorporating battery operating cost,” IEEE Trans. Power Syst., vol. 31, pp. 2289 – 2296, 2015.

Y. Zhang, N. Gatsis, and G. Giannakis, “Robust energy management for microgrids with high-penetration renewables,” IEEE Trans. Sustain. Energy, vol. 4, 2012.

D. Jiang, T. Pham, W. Powell, D. Salas, and W. Scott, “A comparison of approximate dynamic programming techniques on benchmark energy storage problems: Does anything work?” 2014 IEEE Symposium on Adaptive Dynamic Programming and Reinforcement Learning (ADPRL), pp. 1–8, 2014.

P. Zeng, H. Li, H. He, and S. Li, “Dynamic energy management of a microgrid using approximate dynamic programming and deep recurrent neural network learning,” IEEE Trans. Smart Grid, vol. PP, pp. 171–188, 2018.

S. Zhou, Z. Hu, W. Gu, M. Jiang, and X.-P. Zhang, “Artificial intelligence based smart energy community management: A reinforcement learning approach,” CSEE J. Power Energy Syst., vol. 5, 03 2019.

M. N. Alam, S. Chakrabarti, and X. Liang, “A benchmark test system for networked microgrids,” IEEE Trans. Ind. Informat., vol. 16, no. 10, pp. 6217–6230, 2020.

A. G. Barto, S. J. Bradtke, and S. P. Singh, “Learning to act using real-time dynamic programming,” Artif. Intell., vol. 72, no. 1–2, 1995.

C. Essayeh, M. Raiss El-Fenni, and H. Dahmouni, “Towards an intelligent home energy management system for smart microgrid applications,” 2016 International Wireless Communications and Mobile Computing Conference (IWCMC), pp. 1051–1056, 2016.

S. A. Pourmousavi Kani, M. H. Nehrir, and R. Sharma, “Multitimescale power management for islanded microgrids including storage and demand response,” IEEE Trans. Smart Grid, vol. 6, pp. 1185–1195, 2015.

K. Dehghanpour and H. Nehrir, “A market-based resilient power management technique for distribution systems with multiple microgrids using a multi-agent system approach,” Electric Power Comp. Syst., vol. 46, no. 16-17, pp. 1744–1755, 2018.

B. Moran, “Microgrid load management and control strategies,” IEEE/PES Transmission and Distribution Conference and Exposition (T&D), pp. 1–4, 2016.

K. Dehghanpour, M. H. Nehrir, J. W. Sheppard, and N. C. Kelly, “Agent-based modeling of retail electrical energy markets with demand response,” IEEE Trans. Smart Grid, vol. 9, no. 4, pp. 3465–3475, 2018.

R. Bellman, “A markovian decision process,” Journal of Mathematics and Mechanics, vol. 6, no. 5, pp. 679–684, 1957.

E. Alpaydin, Introduction to Machine Learning, 3rd ed. MIT Press, 2014.

C. J. C. H. Watkins, “Learning from delayed rewards,” Ph.D. dissertation, King’s College, Cambridge, UK, 1989.

C. J. Watkins and P. Dayan, “Q-learning,” Machine learning, vol. 8, no. 3-4, pp. 279–292, 1992.

I. T. Force *et al.*, “Trends in Microgrid Control,” vol. 5, no. 4, pp. 1905–1919, 2014.

R. Majumder, “Some Aspects of Stability in Microgrids,” vol. 28, no. 3, pp. 3243–3252, 2013.

Q. C. Zhong and Y. Zeng, “Universal Droop Control of Inverters with Different Types of Output Impedance,” *IEEE Access*, vol. 4, pp. 702–712, 2016.

N. Pogaku, S. Member, M. Prodanovic, T. C. Green, and S. Member, “Modeling, Analysis and Testing of Autonomous Operation of an Inverter Based Microgrid,” vol. 22, no. 2, pp. 613–625, 2007.

I. Chung *et al.*, “Control Methods of Inverter-Interfaced Distributed Generators in a Microgrid System,” vol. 46, no. 3, pp. 1078–1088, 2010.

M. A. Hassan and M. A. Abido, “Optimal Design of Microgrids in Autonomous and Grid-Connected Modes Using Particle Swarm Optimization,” vol. 26, no. 3, pp. 755–769, 2011.

K. Yu, Q. Ai, S. Wang, J. Ni, and T. Lv, “Analysis and Optimization of Droop Controller for Microgrid System Based on Small-Signal Dynamic Model,” vol. 7, no. 2, pp. 695–705, 2016.

J. Hu, J. Zhu, D. G. Dorrell, and J. M. Guerrero, “Virtual flux droop method - A new control strategy of inverters in microgrids,” *IEEE Trans. Power Electron.*, vol. 29, no. 9, pp. 4704–4711, 2014.

D. K. Dheer, N. Soni, and S. Doolla, “Sustainable Energy, Grids and Networks Improvement of small signal stability margin and transient response in inverter-dominated microgrids,” *Sustain Energy, Grids Networks*, vol. 5, pp. 135–147, 2016.

D. K. Dheer, O. V. Kulkarni, S. Doolla, and A. K. Rathore, “Effect of Reconfiguration and Meshed Networks on the Small-Signal Stability Margin of Droop-Based Islanded Microgrids,” *IEEE Trans. Ind. Appl.*, vol. 54, no. 3, pp. 2821–2833, 2018.

I. Chung *et al.*, “Control Methods of Inverter-Interfaced Distributed Generators in a Microgrid System,” vol. 46, no. 3, pp. 1078–1088, 2010.

K. Yu, Q. Ai, S. Wang, J. Ni, and T. Lv, “Analysis and Optimization of Droop Controller for Microgrid System Based on Small-Signal Dynamic Model,” vol. 7, no. 2, pp. 695–705, 2016.

D. K. Dheer, N. Soni, and S. Doolla, “Sustainable Energy, Grids and Networks Improvement of small signal stability margin and transient response in inverter-dominated microgrids,” *Sustain. Energy, Grids Networks*, vol. 5, pp. 135–147, 2016.

D. K. Dheer, S. Doolla, S. Bandyopadhyay, and J. M. Guerrero, “Electrical Power and Energy Systems Effect of placement of droop based generators in distribution network on small signal stability margin and network loss,” *Int. J. Electr. Power Energy Syst.*, vol. 88, pp. 108–118, 2017.

A. Elrayyah, F. Cingoz, Y. Sozer, and S. Member, “Construction of Nonlinear Droop Relations to Optimize Islanded Microgrid Operation,” vol. 51, no. 4, pp. 3404–3413, 2015.

I. A. C. Microgrids *et al.*, “Containment and Consensus-Based Distributed Coordination Control to Achieve Bounded Voltage and Precise Reactive Power Sharing in,” vol. 53, no. 6, pp. 5187–5199, 2017.

N. Bottrell, S. Member, M. Prodanovic, T. C. Green, and S. Member, “Dynamic Stability of a Microgrid With an Active Load,” vol. 28, no. 11, pp. 5107–5119, 2013.

X. Tang, W. Deng, and Z. Qi, “Investigation of the Dynamic Stability of Microgrid,” vol. 29, no. 2, pp. 698–706, 2014.

A. Kahrobaeian, S. Member, Y. A. I. Mohamed, and S. Member, “Analysis and Mitigation of Low-Frequency Instabilities in Autonomous Medium-Voltage Converter-Based Microgrids With Dynamic Loads,” vol. 61, no. 4, pp. 1643–1658, 2014.

E. S. N. P. Raju and T. Jain, “Impact of load dynamics and load sharing among distributed generations on stability and dynamic performance of islanded AC microgrids,” *Electr. Power Syst. Res.*, vol. 157, pp. 200–210, 2018, doi: 10.1016/j.epsr.2017.12.022.

M. Yazdanian and A. Mehrizi-Sani, “Internal model-based current control of the RL filter-based voltage-sourced converter,” *IEEE Trans. Energy Convers.*, vol. 29, no. 4, pp. 873–881, 2014.

S. Leitner, M. Yazdanian, A. Mehrizi-Sani, and A. Muetze, “Small-Signal Stability Analysis of an Inverter-Based Microgrid with Internal Model-Based Controllers,” *IEEE Trans. Smart Grid*, vol. 9, no. 5, pp. 5393–5402, 2018.

M. Rasheduzzaman, J. A. Mueller, and J. W. Kimball, “An accurate small-signal model of inverter-dominated islanded microgrids using (dq) reference frame,” *IEEE J. Emerg. Sel. Top. Power Electron.*, vol. 2, no. 4, pp. 1070–1080, 2014.

Q. Zhong and S. Member, “Robust Droop Controller for Accurate Proportional Load Sharing Among Inverters Operated in Parallel,” vol. 60, no. 4, pp. 1281–1290, 2013.

N. K. Vemula, S. K. Parida, and S. Member, “Small Signal Stability Assessment of an Inverter-Based Microgrid With Universal Droop and Internal Model-Based Controllers.”

L. Lei, M. A. Elgendy, N. Wade, and S. Ethni, “Power sharing between parallel inverters by using droop control with a secondary control loop,” *PEDG 2019 - 2019 IEEE 10th Int. Symp. Power Electron. Distrib. Gener. Syst.*, pp. 653–658, 2019.

V. NARESH KUMAR AND S. K. PARIDA, "PARAMETER OPTIMIZATION OF UNIVERSAL DROOP AND INTERNAL MODEL CONTROLLER FOR MULTI INVERTER-FED DGS BASED ON ACCURATE SMALL-SIGNAL MODEL," IN IEEE ACCESS, VOL. 7, PP. 101928-101940, 2019.

H. M. GOODARZI AND M. H. KAZEMI, “AN OPTIMAL AUTONOMOUS MICROGRID CLUSTER BASED ON DISTRIBUTED GENERATION DROOP PARAMETER OPTIMIZATION AND RENEWABLE ENERGY SOURCES USING AN IMPROVED GREY WOLF OPTIMIZER,” *ENG. OPTIM.*, VOL. 0, NO. 0, PP. 1 21, 2017.

J. POMBO AND M. CALADO, “PROPORTIONAL RESONANT CURRENT CONTROL AND OUTPUT-FILTER DESIGN OPTIMIZATION FOR GRID-TIED INVERTERS USING GREY WOLF OPTIMIZER,” 2020.

A. DJERIOUI, A. HOUARI, M. MACHMOUM, M. GHANES, T. MESBAHI AND M. F. BENKHORIS, "GREY WOLF OPTIMIZER BASED PREDICTIVE TORQUE CONTROL FOR ELECTRIC VEHICLE APPLICATIONS," *2020 22ND EUROPEAN CONFERENCE ON POWER ELECTRONICS AND APPLICATIONS (EPE'20 ECCE EUROPE)*, 2020, PP. P.1-P.5

R. SANJAY, T. JAYABARATHI, T. RAGHUNATHAN, V. RAMESH AND N. MITHULANANTHAN, "OPTIMAL ALLOCATION OF DISTRIBUTED GENERATION USING HYBRID GREY WOLF OPTIMIZER," IN *IEEE ACCESS*, VOL. 5, PP. 14807-14818, 2017

H. A. HASSAN AND M. ZELLAGUI, “APPLICATION OF GREY WOLF OPTIMIZER ALGORITHM FOR OPTIMAL POWER FLOW OF TWOTERMINAL HVDC TRANSMISSION SYSTEM,” PP. 701–712, 2017, DOI: 10.15598/AEEE.V15I5.2110.

M. Farhoodnea, A. Mohamed, H. Shareef, and H. Zayandehroodi, “Power quality impacts of high-penetration electric vehicle stations and renewable energy-based generators on power distribution systems,” Meas. J. Int. Meas. Confed., vol. 46, no. 8, pp. 2423–2434, 2013.

V. H. M. Quezada, J. R. Abbad, and T. G. San Román, “Assessment of energy distribution losses for increasing penetration of distributed generation,” IEEE Trans. Power Syst., vol. 21, no. 2, pp. 533–540, 2006

N. Miller and Z. Ye, “Report on Distributed Generation Penetration Study,” 2003.

NREL, “DG Power Quality, Protection and Reliability Case Studies Report,” 2003.

G. Carpinelli, G. Celli, S. Mocci, F. Mottola, F. Pilo, and D. Proto, “Optimal Integration of Distributed Energy Storage Devices in Smart Grids,” IEEE Trans. Smart Grid, vol. 4, no. 2, pp. 985–995, Jun. 2013.

N. Jayasekara, P. Wolfs, and M. A. S. Masoum, “An optimal management strategy for distributed storages in distribution networks with high penetrations of PV,” Electr. Power Syst. Res., vol. 116, pp. 147–157, Nov. 2014.

H. Nazaripouya, Y. Wang, P. Chu, H. R. Pota, and R. Gadh, “Optimal sizing and placement of battery energy storage in distribution system based on solar size for voltage regulation,” in 2015 IEEE Power & Energy Society General Meeting, 2015, pp. 1–5.

E. Hooshmand and A. Rabiee, “Robust model for optimal allocation of renewable energy sources, energy storage systems and demand response in distribution systems via information gap decision theory,” IET Gener. Transm. Distrib., vol. 13, no. 4, pp. 511–520, 2019.

A. W. Bizuayehu, A. A. Sanchez de la Nieta, J. Contreras, and J. P. S. Catalao, “Impacts of Stochastic Wind Power and Storage Participation on Economic Dispatch in Distribution Systems,” IEEE Trans. Sustain. Energy, vol. 7, no. 3, pp. 1336–1345, Jul. 2016.

A. Karimi, F. Aminifar, A. Fereidunian, and H. Lesani, “Energy storage allocation in wind integrated distribution networks: An MILP-Based approach,” Renew. Energy, vol. 134, pp. 1042–1055, Apr. 2019.

S. Sukumar, H. Mokhlis, S. Mekhilef, K. Naidu, and M. Karimi, “Mix-mode energy management strategy and battery sizing for economic operation of grid-tied microgrid,” Energy, vol. 118, pp. 1322–1333, 2017

A. S. O. Ogunjuyigbe, T. R. Ayodele, and O. A. Akinola, “Optimal allocation and sizing of PV/Wind/Split-diesel/Battery hybrid energy system for minimizing life cycle cost, carbon emission and dump energy of remote residential building,” Appl. Energy, vol. 171, pp. 153–171, 2016

R. V. A. Monteiro, G. C. Guimarães, F. A. M. Moura, M. R. M. C. Albertini, and F. B. Silva, “Long-term sizing of lead–acid batteries in order to reduce technical losses on distribution networks: A distributed generation approach,” Electr. Power Syst. Res., vol. 144, pp. 163–174, 2017

Z. Liu, F. Wen, G. Ledwich, "Optimal siting and sizing of distributed generators in distribution systems considering uncertainties," IEEE Trans. Power Delivery, vol. 26, pp. 2541-2551, Oct. 2011.

Thomas L. Saaty ‘Decision making — the Analytic Hierarchy and Network Processes (AHP/ANP) ‘Journal of Systems Science and Systems Engineering, vol. 13, pp. 1-35, Mar. 2004

M. N. Alam, S. Chakrabarti, and X. Liang, “A Benchmark Test System for Networked Microgrids,” IEEE Trans. Ind. Informatics, vol. 16, no. 10, pp. 6217–6230, 2020